We took advantage of the LacZ allele that was inserted in the *Runx*2 locus in *Runx*2$^{+/-}$ mice. *Runx*2 messenger RNA (mRNA) expression can be monitored by LacZ staining in these mice. Before compression, we were able to observe *Runx*2 mRNA expression in osteoblasts on bone trabeculae and growth-plate chondrocytes, but not in the endplate, demonstrating that expression of *Runx*2 was minimal. Surprisingly, after compression, numerous LacZ-positive cells were observed in the cartilaginous endplate (Figure 5C), thus demonstrating that compression induced *Runx*2 expression.

Up-regulation of Runx2 in human IVD degeneration. Finally, to determine if the induction of Runx2 is also involved in the development of IVD degeneration in humans, we analyzed *Runx*2 mRNA expression in patients with moderate disc degeneration. We collected RNA from the affected IVDs of these patients, and compared the RNA levels with those in intact IVDs as a control. Similar to that observed in the mouse model, expression of *Runx*2 mRNA was up-regulated in all patients with IVD degeneration examined (Figure 5D). Taken together, these results clearly demonstrate that in both mice and humans, IVD degeneration is accompanied by induction of Runx2.

DISCUSSION

On the basis of previous findings showing that Runx2 is an important regulator of chondrocyte hypertrophy, we examined the role of other Runx family members, Runx1 and Runx3, in chondrocytes, particularly in chondrocyte differentiation in vivo, and compared these results with those obtained for Runx2. Overexpression of *Runx*1, *Runx*2, or *Runx*3 in nonhypertrophic chondrocytes led to skeletal abnormalities, indicating that the expression of these genes at precise times during skeletal development and chondrocyte differentiation is important, and that each gene must have a distinct role in the differentiation of chondrocytes.

In addition to the ectopic mineralization observed, overexpression of *Runx*1 or *Runx*2 led to IVD degeneration. We showed that Runx2 is the only family member normally expressed in the IVD, and that Runx2 expression, along with chondrocyte hypertrophy, were induced in a mouse model of IVD degeneration. Finally, we demonstrated that in human patients with IVD degeneration, Runx2 expression was significantly up-regulated, thus suggesting that Runx2 contributes to the pathogenesis of IVD degeneration through the induction of chondrocyte hypertrophy.

In the present study, *Runx*1 expression in WT mice was restricted mostly to progenitor cells that were not yet committed to either the chondrocyte or the osteoblast lineage, a finding consistent with that described in other reports (22,23). Overexpression of *Runx*1 in chondrocytes does not induce any phenotypic abnormalities in the growth-plate chondrocyte, suggesting that Runx1 does not play a major role in the differentiation of these chondrocytes. Interestingly, it has been reported that forced expression of *Runx*1 in mesenchymal cells induced chondrocyte differentiation in vitro (24). This indicates that the function of Runx1 is possibly required only in the very early stages of chondrocyte differentiation. However, because the present study used an α1(II) collagen promoter to drive *Runx*1 expression, and this promoter is active only in cells that have differentiated into chondrocytes, we were precluded from testing this possibility.

Our results also showed that in WT mice, *Runx*3 was expressed in prehypertrophic chondrocytes and, in contrast to *Runx*2, its expression did not decrease throughout embryonic development, suggesting that *Runx*3 may play a role in chondrocyte differentiation after birth (8,9). Previously, Runx3, in conjunction with Runx2, was shown to regulate chondrocyte differentiation, but the neonatal mortality of Runx3-deficient mice hampered any further study of the role of Runx3 in the postnatal period (9). We recently observed that Runx3-deficient mice that survived perinatally exhibited impaired longitudinal growth postnatally (Takeda S, et al: unpublished observations). This observation, together with the ectopic mineralization in α1(II)-*Runx*3 mice, substantiates the physiologic importance of Runx3 in chondrocyte differentiation.

The results from the present study also showed that each member of the Runx family has a distinct ability to drive chondrocyte differentiation in vivo. Notably, only the α1(II)-*Runx*2 mice developed the phenotypes of both ectopic mineralization and IVD degeneration. This ability of Runx2 to induce both intervertebral degeneration and growth-plate chondrocyte differentiation could be attributable to its unique expression pattern or to its ability to recruit specific coregulators. The latter explanation is more likely, since the Runx-transgenic mice had distinct phenotypes despite comparable patterns of expression and comparable levels of each transgene driven by the same promoter cassette in each mouse. Since the runt DNA binding domain was observed to be highly homologous with that in other Runx proteins (Figure 2A), and yet the α1(II)-*Runx*2ΔQA mice still exhibited ectopic chondrocyte differentiation (Figure 2D), it is conceivable that the carboxyl domain

of Runx2 may interact with specific coregulators to induce chondrocyte differentiation.

Indeed, many transcriptional regulators have been found to be associated with the C-terminus of Runx2 (25–29). Of these regulators, Smad3 is the most promising, since Runx2, but not Runx1 or Runx3, has been shown to induce osteocalcin promoter activity, and this was inhibited by activation of transforming growth factor β (TGFβ) or Smad3 (30,31). Moreover, mice that either expressed a dominant-negative form of the TGFβII receptor or were deficient in Smad3 developed accelerated chondrocyte differentiation as well as kyphosis (32,33), which is reminiscent of the phenotype observed in α1(II)-*Runx*2 mice. Therefore, TGFβ/Smad3 signaling and Runx2 may cooperatively regulate chondrocyte differentiation. This hypothesis would be supported if Runx2 activity were shown to be increased either in mice expressing a dominant-negative form of the TGFβII receptor or in mice deficient in Smad3.

The most interesting and unexpected finding in the present study was the observation of IVD degeneration in both α1(II)-*Runx*1 and α1(II)-*Runx*2 mice. IVD degeneration is one of the most common degenerative disorders of the joints (34). Although matrix metalloproteinase 3 and a number of matrix genes, such as type II collagen, type IX collagen, and aggrecan, have been shown to be involved in the pathogenesis of IVD degeneration, the molecular mechanism is still largely unknown.

In this study, we demonstrated that Runx2 is involved in the development of IVD degeneration. There was substantial evidence to support this conclusion. First, overexpression of *Runx*2 or *Runx*1 in cartilaginous endplates induced IVD destruction. Second, weight loading, which is clinically a major cause of IVD degradation, induced expression of *Runx*2, but not that of *Runx*1, in the endplate of WT mice. Third, *Runx*2 expression coincided with the region of degradation of extracellular matrices in WT mice. We showed that Runx2 protein was expressed in older WT mice, but not in young mice; this coincided with the timeframe over which some of the WT mice developed IVD degradation. Finally, *Runx*2 expression was clearly induced in the degraded IVD in human patients.

Notably, the phenotypic abnormalities observed in α1(II)-*Runx*1– or α1(II)-*Runx*2–transgenic mice did not completely recapitulate the phenotype observed in human patients with IVD degeneration. Nevertheless, although the phenotype was much milder in mice with mechanical stress–induced IVD degeneration, it still led to concurrent expression of *Runx*2 in the mice. In fact, histologically, these mice exhibited degenerated nucleus pulposus without IVD height abnormalities, equivalent to the grade 3 to grade 4 IVD degeneration (17) observed in human patients. Collectively, our observations in mice and humans strongly support the hypothesis that Runx2 is intimately involved in IVD degradation and may even physiologically initiate the process.

The molecular mechanism by which mechanical loading induces expression of Runx2 in the IVD is unknown. However, it has been reported that mechanical loading induces Runx2 expression in osteoblasts through the MAP kinase pathway (35), and this same pathway may also be involved in the Runx2 expression observed in IVD degeneration. Given the prevalence of IVD degeneration in humans, an approach involving manipulation of the activity or expression of *Runx*2 or its downstream genes may be an attractive proposition as a novel therapy for these types of conditions.

ACKNOWLEDGMENTS

We would like to thank M. Patel, T. Kato, M. Noda, and U. Chung for helpful discussions and for reading the text. We also thank S. Sunamura and J. Chen for their superb technical assistance, and B. de Crombrugghe for providing the α1(II) collagen promoter and enhancer cassette.

AUTHOR CONTRIBUTIONS

Dr. Takeda had full access to all of the data in the study and takes responsibility for the integrity of the data and the accuracy of the data analysis.

Study design. Takeda.

Acquisition of data. Sato, Kimura, Ozdemir, Asou, Miyazaki, Jinno, Ae, Liu, Osaki, Takeuchi, Fukumoto, Kawaguchi, Haro, Shinomiya, Karsenty.

Analysis and interpretation of data. Takeda.

Manuscript preparation. Takeda.

Statistical analysis. Takeda.

REFERENCES

1. Kronenberg HM. Developmental regulation of the growth plate. Nature 2003;423:332–6.
2. Karsenty G, Wagner EF. Reaching a genetic and molecular understanding of skeletal development [review]. Dev Cell 2002;2: 389–406.
3. Poole AR. The growth plate: cellular physiology, cartilage assembly and mineralization. In: Hall BK, Newman SA, editors. Cartilage: molecular aspects. Boca Raton (FL): CRC Press; 1991. p. 179–211.
4. Bi W, Deng JM, Zhang Z, Behringer RR, de Crombrugghe B. Sox9 is required for cartilage formation. Nat Genet 1999;22:85–9.
5. Akiyama H, Chaboissier MC, Martin JF, Schedl A, de Crombrugghe B. The transcription factor Sox9 has essential roles in successive steps of the chondrocyte differentiation pathway and is required for expression of Sox5 and Sox6. Genes Dev 2002;16: 2813–28.
6. Ueta C, Iwamoto M, Kanatani N, Yoshida C, Liu Y, Enomoto-Iwamoto M, et al. Skeletal malformations caused by overexpres-

sion of Cbfa1 or its dominant negative form in chondrocytes. J Cell Biol 2001;153:87–100.
7. Takeda S, Bonnamy JP, Owen MJ, Ducy P, Karsenty G. Continuous expression of Cbfa1 in nonhypertrophic chondrocytes uncovers its ability to induce hypertrophic chondrocyte differentiation and partially rescues Cbfa1-deficient mice. Genes Dev 2001;15: 467–81.
8. Stricker S, Fundele R, Vortkamp A, Mundlos S. Role of Runx genes in chondrocyte differentiation. Dev Biol 2002;245:95–108.
9. Yoshida CA, Yamamoto H, Fujita T, Furuichi T, Ito K, Inoue K, et al. Runx2 and Runx3 are essential for chondrocyte maturation, and Runx2 regulates limb growth through induction of Indian hedgehog. Genes Dev 2004;18:952–63.
10. Ito Y, Miyazono K. RUNX transcription factors as key targets of TGF-β superfamily signaling. Curr Opin Genet Dev 2003;13:43–7.
11. Thirunavukkararsu K, Mahajan M, McLarren KW, Stifani S, Karsenty G. Two domains unique to the osteoblast-specific transcription factor Osf2/Cbfa1 contribute to its transactivation function and its inability to heterodimerize with Cbfβ. Mol Cell Biol 1998;18:4197–208.
12. Otto F, Thornell AP, Crompton T, Denzel A, Gilmour KC, Rosewell IR, et al. Cbfa1, a candidate gene for cleidocranial dysplasia syndrome, is essential for osteoblast differentiation and bone development. Cell 1997;89:765–71.
13. Van der Kraan PM, Vitters EL, van Beuningen HM, van de Putte LB, van den Berg WB. Degenerative knee joint lesions in mice after a single intra-articular collagenase injection: a new model of osteoarthritis. J Exp Pathol (Oxford) 1990;71:19–31.
14. Planaguma J, Diaz-Fuertes M, Gil-Moreno A, Abal M, Monge M, Garcia A, et al. A differential gene expression profile reveals overexpression of RUNX1/AML1 in invasive endometrioid carcinoma. Cancer Res 2004;64:8846–53.
15. Osaki M, Moriyama M, Adachi K, Nakada C, Takeda A, Inoue Y, et al. Expression of RUNX3 protein in human gastric mucosa, intestinal metaplasia and carcinoma. Eur J Clin Invest 2004;34: 605–12.
16. Lotz JC, Colliou OK, Chin JR, Duncan NA, Liebenberg E. Compression-induced degeneration of the intervertebral disc: an in vivo mouse model and finite-element study. Spine 1998;23: 2493–506.
17. Pfirrmann CW, Metzdorf A, Zanetti M, Hodler J, Boos N. Magnetic resonance classification of lumbar intervertebral disc degeneration. Spine 2001;26:1873–8.
18. Mundlos S. Expression patterns of matrix genes during human skeletal development. Prog Histochem Cytochem 1994;28:1–47.
19. Zhou G, Lefebvre V, Zhang Z, Eberspaecher H, de Crombrugghe B. Three high mobility group-like sequences within a 48-base pair enhancer of the Col2a1 gene are required for cartilage-specific expression in vivo. J Biol Chem 1998;273:14989–97.
20. McLeod MJ. Differential staining of cartilage and bone in whole mouse fetuses by alcian blue and alizarin red S. Teratology 1980;22:299–301.
21. Urban JP, Roberts S. Degeneration of the intervertebral disc. Arthritis Res Ther 2003;5:120–30.
22. Smith N, Dong Y, Lian JB, Pratap J, Kingsley PD, van Wijnen AJ, et al. Overlapping expression of Runx1(Cbfa2) and Runx2(Cbfa1) transcription factors supports cooperative induction of skeletal development. J Cell Physiol 2005;203:133–43.
23. Yamashiro T, Aberg T, Levanon D, Groner Y, Thesleff I. Expression of Runx1, -2 and -3 during tooth, palate and craniofacial bone development. Mech Dev 2002;119 Suppl 1:S107–10.
24. Wang Y, Belflower RM, Dong YF, Schwarz EM, O'Keefe RJ, Drissi H. Runx1/AML1/Cbfa2 mediates onset of mesenchymal cell differentiation toward chondrogenesis. J Bone Miner Res 2005;20: 1624–36.
25. Xiao G, Jiang D, Ge C, Zhao Z, Lai Y, Boules H, et al. Cooperative interactions between activating transcription factor 4 and Runx2/Cbfa1 stimulate osteoblast-specific osteocalcin gene expression. J Biol Chem 2005;280:30689–96.
26. Wang W, Wang YG, Reginato AM, Glotzer DJ, Fukai N, Plotkina S, et al. Groucho homologue Grg5 interacts with the transcription factor Runx2-Cbfa1 and modulates its activity during postnatal growth in mice. Dev Biol 2004;270:364–81.
27. Gutierrez S, Javed A, Tennant DK, van Rees M, Montecino M, Stein GS, et al. CCAAT/enhancer-binding proteins (C/EBP) β and δ activate osteocalcin gene transcription and synergize with Runx2 at the C/EBP element to regulate bone-specific expression. J Biol Chem 2002;277:1316–23.
28. Thomas DM, Carty SA, Piscopo DM, Lee JS, Wang WF, Forrester WC, et al. The retinoblastoma protein acts as a transcriptional coactivator required for osteogenic differentiation. Mol Cell 2001; 8:303–16.
29. Zhang YW, Yasui N, Ito K, Huang G, Fujii M, Hanai J, et al. A RUNX2/PEBP2α A/CBFA1 mutation displaying impaired transactivation and Smad interaction in cleidocranial dysplasia. Proc Natl Acad Sci U S A 2000;97:10549–54.
30. Alliston T, Choy L, Ducy P, Karsenty G, Derynck R. TGF-β-induced repression of CBFA1 by Smad3 decreases cbfa1 and osteocalcin expression and inhibits osteoblast differentiation. EMBO J 2001;20:2254–72.
31. Kang JS, Alliston T, Delston R, Derynck R. Repression of Runx2 function by TGF-β through recruitment of class II histone deacetylases by Smad3. EMBO J 2005;24:2543–55.
32. Serra R, Johnson M, Filvaroff EH, LaBorde J, Sheehan DM, Derynck R, et al. Expression of a truncated, kinase-defective TGF-β type II receptor in mouse skeletal tissue promotes terminal chondrocyte differentiation and osteoarthritis. J Cell Biol 1997; 139:541–52.
33. Yang X, Chen L, Xu X, Li C, Huang C, Deng CX. TGF-β/Smad3 signals repress chondrocyte hypertrophic differentiation and are required for maintaining articular cartilage. J Cell Biol 2001;153: 35–46.
34. Powell MC, Wilson M, Szypryt P, Symonds EM, Worthington BS. Prevalence of lumbar disc degeneration observed by magnetic resonance in symptomless women. Lancet 1986;2:1366–7.
35. Ziros PG, Gil AP, Georgakopoulos T, Habeos I, Kletsas D, Basdra EK, et al. The bone-specific transcriptional regulator Cbfa1 is a target of mechanical signals in osteoblastic cells. J Biol Chem 2002;277:23934–41.

THE JOURNAL OF BIOLOGICAL CHEMISTRY VOL. 283, NO. 36, pp. 24682–24689, September 5, 2008

Krüppel-like Factor 5 Causes Cartilage Degradation through Transactivation of Matrix Metalloproteinase 9*[S]

Received for publication, December 3, 2007, and in revised form, June 23, 2008 Published, JBC Papers in Press, July 10, 2008, DOI 10.1074/jbc.M709857200

Yusuke Shinoda[‡], Naoshi Ogata[§], Akiro Higashikawa[‡], Ichiro Manabe[¶], Takayuki Shindo[¶], Takashi Yamada[‡], Fumitaka Kugimiya[‡], Toshiyuki Ikeda[§], Naohiro Kawamura[‡], Yosuke Kawasaki[‡], Kensuke Tsushima[¶], Norifumi Takeda[¶], Ryozo Nagai[¶], Kazuto Hoshi[‡], Kozo Nakamura[‡], Ung-il Chung[§], and Hiroshi Kawaguchi[‡1]

From [‡]Sensory and Motor System Medicine, [¶]Circulatory Medicine, and [§]Bone and Cartilage Regeneration Medicine, University of Tokyo, Tokyo 113-8655, Japan

Although degradation of cartilage matrix has been suggested to be a rate-limiting step for endochondral ossification during skeletal development, little is known about the transcriptional regulation. This study investigated the involvement of KLF5 (Krüppel-like factor 5), an Sp/KLF family member, in the skeletal development. KLF5 was expressed in chondrocytes and osteoblasts but not in osteoclasts. The heterozygous deficient ($KLF5^{+/-}$) mice exhibited skeletal growth retardation in the perinatal period. Although chondrocyte proliferation and differentiation were normal, cartilage matrix degradation was impaired in $KLF5^{+/-}$ mice, causing delay in replacement of cartilage with bone at the primary ossification center in the embryonic limbs and elongation of hypertrophic chondrocyte layer in the neonatal growth plates. Microarray analyses identified MMP9 (matrix metalloproteinase 9) as a transcriptional target, since it was strongly up-regulated by adenoviral transfection of KLF5 in chondrogenic cell line OUMS27. The KLF5 overexpression caused gelatin degradation by stimulating promoter activity of MMP9 without affecting chondrocyte differentiation or vascular endothelial growth factor expression in the culture of chondrogenic cells; however, in osteoclast precursors, it affected neither MMP9 expression nor osteoclastic differentiation. KLF5 dysfunction by genetic heterodeficiency or RNA interference was confirmed to cause reduction of MMP9 expression in cultured chondrogenic cells. MMP9 expression was decreased in the limbs of $KLF5^{+/-}$ embryos, which was correlated with suppression of matrix degradation, calcification, and vascularization. We conclude that KLF5 causes cartilage matrix degradation through transcriptional induction of MMP9, providing the first evidence that transcriptional regulation of a proteinase contributes to endochondral ossification and skeletal development.

Endochondral ossification is an essential process for skeletal development and growth (1). During the process, chondrocytes undergo proliferation and hypertrophic differentiation. The hypertrophic chondrocytes then secrete a specialized extracellular matrix rich in type X collagen (COL10),[2] which is replaced by bone matrix. The ossification begins with chondrocyte apoptosis, cartilage matrix degradation, calcification, vascular invasion from perichondrium and bone marrow, and deposition of bone matrix by osteoblasts (2). Among these individual steps, previous studies have indicated that degradation of cartilage matrix is particularly crucial (3–6). This step requires proteolytic breakdown by a variety of proteinases, among which members of the matrix metalloproteinase (MMP) family are of special interest due to their ability to cleave collagens and aggrecan, the two principal matrix components of cartilage (7, 8). However, little is known about transcriptional regulation of MMPs in the endochondral ossification process.

Members of the Krüppel-like factor (KLF) family are important transcription factors that regulate development, cellular differentiation and growth, and pathogenesis of atherosclerosis and tumor development, by controlling the expression of a large number of genes with GC/GT-rich promoters (9). There are currently 17 known members of the mammalian KLF family (10), each of which has individually important biological functions (11). Among the members, KLF5 (IKLF, BTEB2) was identified as a positive regulator of SMemb, a marker gene for activated smooth muscle cells in vascular disease (12). KLF5 shows temporal changes in expression during embryogenesis, with diverse functions in cell differentiation and embryonic development (13, 14). Although KLF5 homozygous knock-out ($KLF5^{-/-}$) mice die *in utero* before embryonic day 8.5 (E8.5), the heterozygous knock-out ($KLF5^{+/-}$) mice are apparently normal and fertile (15). Further analyses of these mice revealed that KLF5 mediates cardiovascular remodeling, since the mice exhibited attenuated cardiac hypertrophy and fibrosis as well as much less granulation formation in response to vascular injury (15). The neonatal $KLF5^{+/-}$ mice also exhibited a marked deficiency in white adipose tissue development, suggesting a contribution to adipogenesis (16).

The KLF family shares similar zinc finger structures with the Sp family, some members of which are known to be essential for

* This work was supported by Grants-in-aid for Scientific Research 16659401 and 18209047 from the Japanese Ministry of Education, Culture, Sports, Science, and Technology. The costs of publication of this article were defrayed in part by the payment of page charges. This article must therefore be hereby marked "*advertisement*" in accordance with 18 U.S.C. Section 1734 solely to indicate this fact.

[S] The on-line version of this article (available at http://www.jbc.org) contains supplemental Tables 1 and 2 and Figs. 1–5.

[1] To whom correspondence should be addressed. Tel.: 81-33815-5411 (ext. 30473); Fax: 81-33818-4082; E-mail: kawaguchi-ort@h.u-tokyo.ac.jp.

[2] The abbreviations used are: COL10, type X collagen; COL2, type II collagen; KLF, Krüppel-like factor; M-CSF, macrophage-colony stimulation factor; M-BMMΦ, M-CSF dependent-bone marrow macrophages; MMP, matrix metalloproteinase; TRAP, tartrate-resistant acid phosphate; RANKL, receptor activator of nuclear factor κB ligand; HE, hematoxylin and eosin; TUNEL, terminal dUTP nick-end labeling; EV, empty vector; RT, reverse transcription; VEGFA, vascular endothelial growth factor A; E*n*, embryonic day *n*; ADAMTS, a disintegrin and metalloproteinase with thrombospondin-like repeat.

skeletal development and growth. For example, Sp3 and Sp7 (osterix) are required for skeletal ossification (17) and osteoblast differentiation (18), respectively. The present study initially detected KLF5 expression in cells of bone and cartilage. To learn the role of KLF5, we analyzed the skeleton of KLF5$^{+/-}$ mice and found that the KLF5 insufficiency caused impaired degradation of cartilage matrix in the perinatal period. We further investigated the underlying molecular mechanisms.

EXPERIMENTAL PROCEDURES

Mice—Generation of KLF5$^{+/-}$ mice was described previously (15). All mice were maintained in the C57BL/6 background with a standard diet. In each experiment, male mice of KLF5$^{+/-}$ and the wild-type littermates were compared. All experiments were performed according to the protocol approved by the Animal Care and Use Committee of the University of Tokyo.

Cell Cultures—Mouse osteoblastic cell line MC3T3-E1, mouse chondrogenic cell line ATDC5, and mouse monocyte-macrophagic cell line RAW264.7 were purchased from RIKEN. Human chondrogenic cell line OUMS27 was purchased from the Health Science Research Resources Bank. For isolation of primary osteoblasts, calvariae of neonatal wild-type mice were digested for 10 min at 37 °C in an enzyme solution containing 0.1% collagenase and 0.2% dispase five times, and cells isolated by the last four digestions were combined. Primary chondrocytes were prepared from ventral rib cages (excluding the sternum) of E18.5 wild-type mouse embryos as previously described (19). For mature osteoclasts, macrophage colony-stimulating factor (M-CSF)-dependent bone marrow macrophages (M-BMMΦ), which are known to be osteoclast precursors, were isolated from bone marrow of 6–8-week-old mice, as previously described (20), and cultured in the presence of M-CSF (30 ng/ml) and soluble receptor activator of nuclear factor κB ligand (RANKL; 100 ng/ml) for 3 days. Primary osteoblasts and MC3T3-E1 cells were cultured in α-minimal essential medium containing 10% fetal bovine serum. Primary chondrocytes, ATDC5, OUMS27, and Raw264.7 cells were cultured in Dulbecco's modified Eagle's medium containing 10% FBS. For proliferation assay of primary chondrocytes, cell number was counted using Cell Counting Kit-8 (Dojindo).

Histological Analyses—The whole skeletons of wild-type and KLF5$^{+/-}$ littermate embryos (E16.5) were fixed in 99.5% ethanol, transferred to acetone, and stained in a solution containing Alizarin red S and Alcian blue 8GX (Sigma). Tibial limbs were fixed in 4% paraformaldehyde/PBS, embedded in paraffin, sectioned in 5-μm slices, and stained with hematoxylin and eosin (HE), toluidine blue, Safranin-O, and 5% silver nitrate (von Kossa), according to the standard procedures. TUNEL staining was performed using an apoptosis *in situ* detection kit (Wako), according to the manufacturer's instruction. TRAP-positive cells were stained at pH 5.0 in the presence of L-(+)-tartaric acid using naphthol AS-MX phosphate in *N,N*-dimethyl formamide as the substrate. For immunohistochemistry, rabbit anti-mouse antibodies against KLF5 (1:100; KM1785) (15), type II collagen (COL2) (1:1000; LSL), COL10 (1:1000; LSL), and osteopontin (1:1000; LSL), a goat anti-mouse antibody against MMP9 (1:150; R&D), a mouse anti-mouse antibody against the aggrecan DIPEN neoepitope (1:100; ab3777; Abcam), and a rat anti-mouse antibody against CD34 clone MEC14.7 (1:50; Hycult Biotech) were used. For bromodeoxyuridine labeling, animals were injected intraperitoneally with bromodeoxyuridine (25 μg/g body weight; Sigma) 2 h prior to sacrifice, and the sections were stained with a bromodeoxyuridine staining kit (Zymed) according to the manufacturer's instructions.

Viral Transfections and Osteoclastogenesis Assay—For adenovirus infection of KLF5 to OUMS27 cells, the construction of adenovirus KLF5 expression vector was described previously (21). Adenovirus expressing KLF5 or the control empty vector (EV) was transduced to the cells at 40 or 100 multiplicities of infection. At 72 h after transfection, the cells were harvested and used for subsequent assays. For retrovirus infection of KLF5 to M-BMMΦ, the construction of retrovirus KLF5 expression vector was described previously (16). M-BMMΦ were infected with KLF5 or control retroviral particles and further cultured with M-CSF (30 ng/ml) and soluble RANKL (100 ng/ml) for 4–5 additional days, and then the number of cells positively stained for TRAP and containing more than three nuclei were counted as osteoclasts.

RNA Interference—Small interfering RNA oligonucleotides were constructed by DHARMACON. They were transfected to OUMS27 cells in concentrations of 200 nM, according to the manufacturer's instructions, and cultured for 72 h for subsequent assays. Small interfering RNA probe sequences are described in the supplemental materials.

Real Time RT-PCR, Western Blotting, and Gelatin Zymography—For RT-PCR, total RNAs were reverse-transcribed with MultiScribe reverse transcriptase (ABI). Real time PCR was performed on an ABI Prism 7000 sequence detection system (ABI) using QuantiTect SYBR Green PCR Master Mix (Qiagen), according to the manufacturer's instructions. Sequence information is described in the supplemental materials. For Western blot analysis, primary antibody to KLF5 (1:1000; KM1785) (15), MMP9 (1:1000; R&D), or β-actin (1:2000; Sigma) was used. For gelatin zymography, 10 μg of cell lysates was loaded to a zymogram acrylamide gel. The gel was electrophophoresed and incubated with developing buffer for 40 h using a Zymography Electrophoresis kit (Cell Garage).

Microarray Analysis—Target genes of KLF5 were identified by comparing mRNA expression in OUMS27 cells with adenoviral introduction of KLF5 or EV using two systems of microarray analyses: APHS-016 (for human extracellular matrix and adhesion molecules; supplemental Table 1) and APHS-024 (for human angiogenesis molecules; supplemental Table 2) in an RT2 Profiler PCR Array System (Super Array Bioscience). For MMP19 and -20 and ADAMTS4, -5, -9, and -15, which are not included in the array systems, real time RT-PCR analysis was separately performed. Sequence information is described in the supplemental materials.

Luciferase Assay—The human MMP9 promoter regions from −1,250 bp relative to the transcriptional start site were cloned into the pGL4-Basic vector (Promega). The luciferase assay was performed with a dual luciferase reporter assay system (Promega) using GloMax™ 96 Microplate Luminometer (Promega).

Radiological Analyses—Plain radiographs were taken using a soft x-ray apparatus (CMB-2, SOFTEX), and bone mineral density was measured by dual energy x-ray absorptiometry using a bone mineral analyzer (PIXImus, Lunar Corp.).

Bone Fracture Experiment—A transverse osteotomy was created at the midshaft of the right tibia using a bone saw and was internally stabilized with an intramedullary nail using the inner pin of a spinal needle of 22- or 23-gauge diameter depending on the size of the cavity, as we reported previously (22, 23). For histological analyses, specimens of the harvested tibias were fixed with 4% paraformaldehyde, decalcified with EDTA, dehydrated with ethanol, embedded in paraffin, and cut into 5-μm sections. The sections were stained with HE or toluidine blue.

Arthritis Experiment—Arthritis was induced by the modified method of Terato *et al.* (24, 25). Briefly, mice were injected intraperitoneally with 10 mg of an anti-COL2 monoclonal antibody (Immuno-Biological Laboratory) on day 0. On days 2 and 7, 50 μg of lipopolysaccharide (100 μl of 500 μg/ml solution in saline) was injected intraperitoneally, followed by an intermittent lipopolysaccharide injection every 3 days to the end of the experiment. As a control, 2.5 and 0.1 ml of saline was injected similarly to the antibody and lipopolysaccharide, respectively. The clinical severity of arthritis was graded on a 0–3 scale as follows: 0, normal; 1, swelling of ankle or wrist or limited to digits; 2, swelling of the entire paw; 3, maximal swelling. Each limb was graded by a single blinded observer, allowing a maximum arthritis score of 12 for each animal.

Statistical Analysis—Means of groups were compared by analysis of variance, and significance of differences was determined by *post hoc* testing using Bonferroni's method.

RESULTS

KLF5 Expression in Bone and Cartilage—To know the involvement of KLF5 in skeletal metabolism, we initially examined the expression of KLF5 mRNA in cells of bone and cartilage by RT-PCR analysis (Fig. 1*A* and supplemental Fig. 1*A*). It was expressed in primary osteoblasts and chondrocytes derived from mouse neonatal calvaria and costal cartilage, respectively, as well as in osteoblastic cell line MC3T3E1 and chondrogenic cell lines ATDC5 and OUMS27. Meanwhile, the expression was hardly detected in osteoclasts formed from the precursor M-BMMΦ (20) or in monocyte-macrophagic cell line RAW264.7. Immunohistochemical analysis of tibial limbs of mouse embryos and neonates showed extensive expression of KLF5 in cells of all layers of cartilage and perichondrium as well as in osteoblasts on primary spongiosa (Fig. 1*B*). The expression in chondrocytes of limb cartilage was visible as early as E13.5 (supplemental Fig. 1*B*).

Impaired Cartilage Degradation and Remodeling in KLF5$^{+/-}$ Limbs—To learn the physiological function of KLF5 *in vivo*, we investigated the skeletal phenotype of KLF5$^{+/-}$ mice, because KLF5$^{-/-}$ mice died before E8.5 (15). Although KLF5$^{+/-}$ embryos (E16.5) showed normal skeletal patterning without abnormality in major organ development, they were smaller in size compared with wild-type littermates (Figs. 2, *A* and *B*). The femoral and tibial limbs of KLF5$^{+/-}$ embryos were 10–15% shorter than those of the wild-type littermates. In the KLF5$^{+/-}$ limb shaft, formation of bone and bone marrow tissues around the primary ossification center was delayed (Fig. 2*B*), and cartilage matrix like COL2 or COL10 remained undegraded in the shaft (Fig. 2*C*). Accordingly, TUNEL-positive apoptotic chondrocytes and tartrate-resistant acid phosphatase (TRAP)-positive osteoclasts/chondroclasts were decreased in the KLF5$^{+/-}$ limb. In the growth plate of neonates, although there was no difference in proliferative and prehypertrophic layers between the genotypes, the hypertrophic layer was elongated in KLF5$^{+/-}$ mice (Fig. 2, *D* and *E*). The Safranin-O-positive proteoglycan matrix remained in the hypertrophic layer, whereas the von Kossa-positive calcification layer was reduced in the KLF5$^{+/-}$ growth plate. These results indicate that the KLF5 insufficiency causes impairment of cartilage degradation and calcification in the perinatal period.

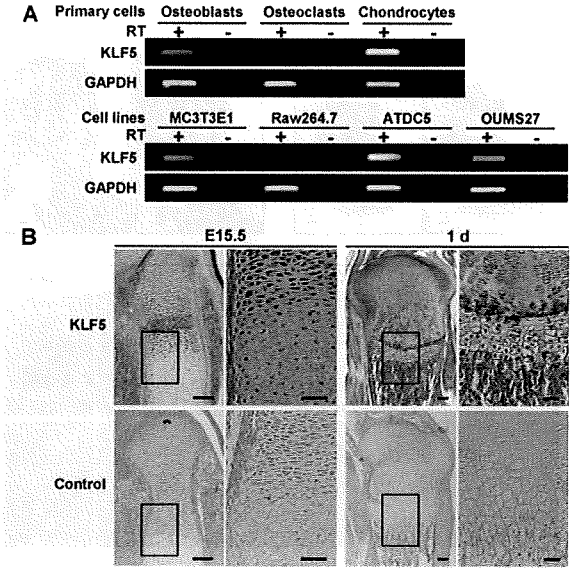

FIGURE 1. **Expression of KLF5 in cells of bone and cartilage.** *A*, mRNA expression of KLF5 and glyceraldehyde 3-phosphate dehydrogenase (*GAPDH*) as the loading control, determined by RT-PCR in mouse primary cells (*upper lanes*) (neonatal calvarial osteoblasts, mature osteoclasts formed from M-BMMΦ with M-CSF and RANKL stimulation, and neonatal costal chondrocytes) and cell lines (*lower lanes*) (osteoblastic cell line MC3T3E1, monocyte-macrophagic cell line Raw264.7, and chondrogenic cell lines ATDC5 and OUMS27). *B*, localization of KLF5 determined by immunohistochemistry by an antibody to KLF5 or the control nonimmune serum in tibial limbs of mouse embryo (E15.5) and neonate (1 day). The *inset boxes* in the *left panels* indicate the regions of the respective *right panels*. *Scale bars*, 100 and 50 μm in *left* and *right panels*, respectively.

In an earlier period prior to the occurrence of ossification in the limb shaft of wild-type mice (E15.5), the limbs were filled with chondrocytes with comparable production of proteoglycan, COL10, and osteopontin in KLF5$^{+/-}$ and the wild-type littermates, indicating that KLF5 insufficiency did not affect chondrocyte differentiation in early stages up to hypertrophic differentiation (supplemental Fig. 2*A*). Chondrocyte proliferation determined by bromodeoxyuridine uptake was also similar between the genotypes (supplemental Fig. 2*B*).

After birth, skeletal growth of KLF5$^{+/-}$ mice caught up with that of wild type, and they became comparable at 4 weeks of age (supplemental Fig. 3, *A* and *B*). KLF5 did not affect bone remodeling after birth either, since bone density of KLF5$^{+/-}$ long bones was normal (supplemental Fig. 3, *C* and *D*).

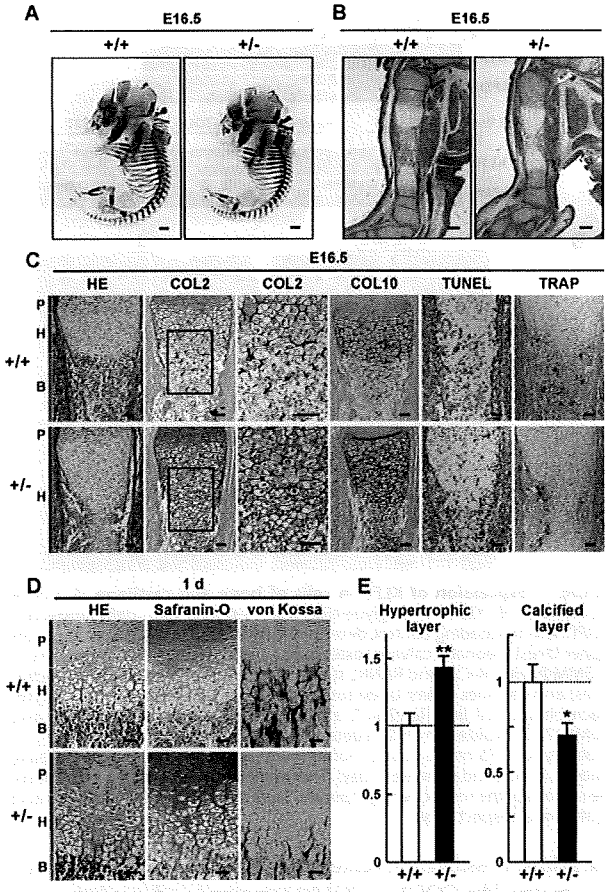

FIGURE 2. **Skeletal phenotypes of KLF5$^{+/-}$ mice in the perinatal period.** *A*, skeletal staining with Alizarin red and Alcian blue; *B*, HE staining of the tibial limbs of wild-type (+/+) and KLF5$^{+/-}$ embryos (E16.5). *Scale bars*, 1 mm and 200 μm, respectively. *C*, HE, COL2, and COL10 immunostainings and TUNEL and TRAP stainings of the tibial limbs of wild-type and KLF5$^{+/-}$ embryos (E16.5). *Inset boxes* in the *left COL2 panels* indicate the regions of the respective *right COL2 panels*. *Blue*, *red*, and *green bars* indicate proliferative (*P*) and hypertrophic (*H*) layers and bone area (*B*), respectively. *Scale bars*, 50 μm. *D*, HE, Safranin-O, and von Kossa stainings of the growth plates in proximal tibias of wild-type and KLF5$^{+/-}$ neonates (1 day). *Scale bars*, 50 μm. *E*, relative lengths of hypertrophic layer (*left*) and calcified layer (*right*) in KLF5$^{+/-}$ growth plate compared with those in wild type (1 day). Data are expressed as means (*bars*) ± S.E. (*error bars*) for 4 mice/group. *, $p < 0.05$; **, $p < 0.01$ *versus* wild type.

MMP9 as a Transcriptional Target of KLF5 in Chondrocytes—To know the molecular mechanism whereby KLF5 contributes to cartilage degradation, we searched for the transcriptional targets by comparing mRNA levels in human chondrogenic cell line OUMS27 adenovirally transfected with KLF5 and the empty vector using microarray and real time RT-PCR analyses (Table 1). Among molecules related to matrix degradation, MMP9 expression was most strongly up-regulated by the KLF5 overexpression.

MMP9 mRNA level was confirmed to be increased in a dose-dependent manner of adenoviral KLF5 overexpression in OUMS27 cells (Fig. 3*A*). In addition, gelatin zymography revealed an increase of gelatin degradation by KLF5, which was compatible with MMP9 activity but not with MMP2 activity, indicating that KLF5 exhibited proteinase activity via the

TABLE 1

Changes in expression of genes related to matrix degradation by KLF5 overexpression

mRNA levels in OUMS27 cells with adenoviral introduction of KLF5 and the control empty vector were compared by RT2 profiler PCR array (APHS-016; SuperArray Bioscience). For MMP19 and -20 and ADAMTS4, -5, -9, and -15, real time RT-PCR was performed using primer sets shown in the supplemental materials. ND, not detected.

Gene symbol	GenBank™ accession number	Increase
		-fold
MMP1	NM_002421	3.1
MMP2	NM_004530	1.6
MMP3	NM_002422	−1.3
MMP7	NM_002423	−1.4
MMP8	NM_002424	2.1
MMP9	NM_004994	2,143.9
MMP10	NM_002425	−1.1
MMP11	NM_005940	−1.8
MMP12	NM_002426	1.4
MMP13	NM_002427	−2.1
MMP14	NM_004995	2.6
MMP15	NM_002428	3.9
MMP16	NM_005941	−1.6
MMP19	NM_002429	1.6
MMP20	NM_004771	ND
ADAMTS1	NM_006988	−2.5
ADAMTS4	NM_005099	46.6
ADAMTS5	NM_007038	−1.4
ADAMTS8	NM_007037	8.4
ADAMTS9	NM_182920	1.1
ADAMTS13	NM_139028	1.6
ADAMTS15	NM_139055	3.1
TIMP1	NM_003254	3.0
TIMP2	NM_003255	3.8
TIMP3	NM_000362	7.7

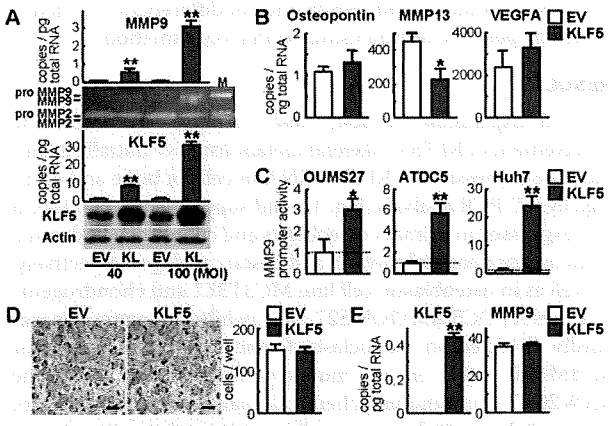

FIGURE 3. **Induction of MMP9 by KLF5 overexpression.** *A*, MMP9 and KLF5 mRNA levels determined by real time RT-PCR analysis after a 3-day culture of human chondrogenic OUMS27 cells adenovirally transfected with empty vector (*EV*) or KLF5 (*KL*) at 40 or 100 multiplicities of infection (*graphs*). Gelatinase activity was determined by gelatin zymography. The *right lane* (*M*) shows markers using recombinant proteins of pro-MMP9, pro-MMP2, and MMP2. KLF5 and actin protein levels were determined by Western blotting. *B*, osteopontin, MMP13, and VEGFA mRNA levels were determined by real time RT-PCR analysis in a 3-day culture of OUMS27 cells adenovirally transfected with 100 multiplicities of infection of EV or KLF5. *C*, MMP9 promoter activity determined by luciferase assay in OUMS27, ATDC5, and Huh7 cells co-transfected with a reporter construct containing the 1,250-bp MMP9 5′-end-flanking region and plasmid vector of EV or KLF5. Data are expressed as relative values compared with EV. *D*, TRAP staining of the osteoclast precursor M-BMMΦ that were retrovirally transfected with EV or KLF5 and cultured with M-CSF and RANKL for 4–5 days. *Scale bars*, 100 μm. The *graph* shows the number of TRAP-positive multinucleated osteoclasts. *E*, mRNA levels of KLF5 and MMP9 determined by real time RT-PCR analysis in the M-BMMΦ cultures. Data are expressed as means (*bars*) ± S.E. (*error bars*). *, $p < 0.05$; **, $p < 0.01$ *versus* EV.

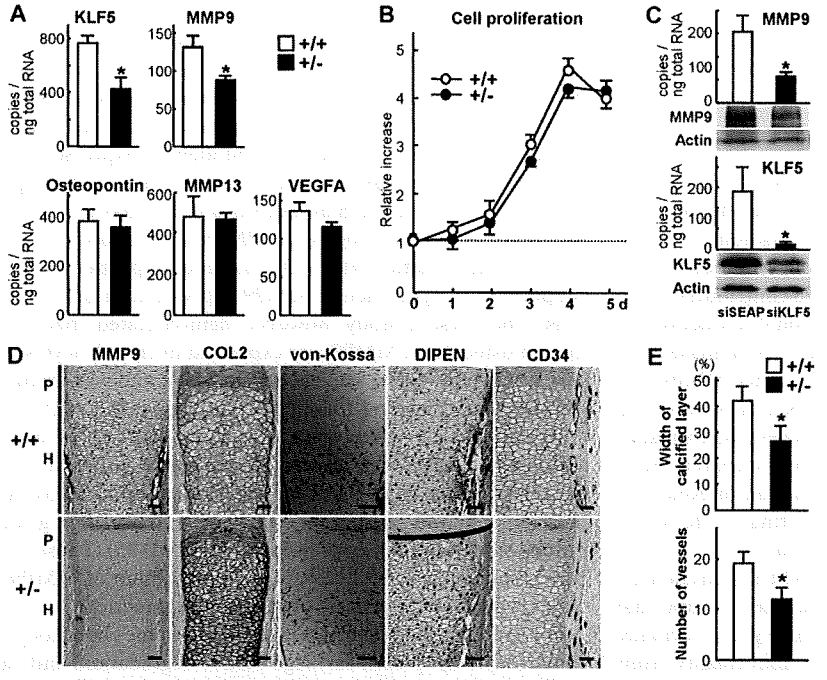

FIGURE 4. **Suppression of MMP9 by KLF5 insufficiency.** *A*, KLF5, MMP9, osteopontin, MMP13, and VEGFA mRNA levels determined by real time RT-PCR analysis in a 3-day culture of primary costal chondrocytes isolated from wild-type (+/+) and KLF5$^{+/-}$ littermates. Data are expressed as means (*bars*) ± S.E. (*error bars*) for 4 mice/group. *, $p < 0.05$ *versus* wild type. *B*, time course of the number of the primary costal chondrocytes above during 5 days of culture. Data are expressed as means (*symbols*) ± S.E. (*error bars*) of the ratios of day 0 for 3 wells/group. *C*, MMP9 and KLF5 mRNA levels determined by real time RT-PCR analysis after a 3-day culture of OUMS27 cells transfected with siSEAP (secreted form of the human placental alkaline phosphatase; control) or siKLF5 oligonucleotides (*graphs*). Data are expressed as means (*bars*) ± S.E. (*error bars*) for 3 wells/group. *, $p < 0.05$ *versus* siSEAP. MMP9, KLF5, and actin protein levels were determined by Western blotting. *D*, MMP9, COL2, DIPEN, and CD34 immunostainings and von Kossa staining of the tibial limbs of E15.5 wild-type and KLF5$^{+/-}$ embryos. *Blue* and *red bars* indicate proliferative (*P*) and hypertrophic (*H*) layers, respectively. *Scale bars*, 50 μm. *E*, the percentage width of the calcified layer to the entire hypertrophic layer determined by the von Kossa staining (*top*) and the number of blood vessels around the hypertrophic layer determined by the CD34 immunostaining (*bottom*) in the growth plates of E15.5 wild-type and KLF5$^{+/-}$ embryos. Data are expressed as means (*bars*) ± S.E. (error bars) for 3 mice/group. *, $p < 0.05$ *versus* wild type.

induction of MMP9. Contrarily, osteopontin mRNA level was not altered by the overexpression, suggesting that chondrocyte differentiation at later stages was not affected by KLF5 (Fig. 3*B*). MMP13 was moderately decreased, whereas vascular endothelial growth factor A (VEGFA) was little regulated by KLF5 in OUMS27 cells, both of which were consistent with the results of microarray analyses (Table 1 and supplemental Tables 1 and 2). To examine the transcriptional regulation, a luciferase reporter gene construct of the MMP9 5′-end-flanking region was transfected into OUMS27, ATDC5, and human hepatocytic Huh7 cells. The transcriptional activity determined by the luciferase reporter assay was enhanced by co-transfection with KLF5 in all cells, demonstrating the transcriptional induction of MMP9 by KLF5 (Fig. 3*C*).

The expression patterns of KLF5 and MMP-9 during chondrocyte differentiation were confirmed to be similar in cultured OUMS-27 cells (supplemental Fig. 1*A*). In addition, the time course analyses by immunostainings of embryonic limbs showed that KLF5 expression was seen early from E13.5, whereas MMP9 expression could be detected at E15.5 and enhanced at E16.5 (supplemental Fig. 1*B*). Since the embryonic stage when the suppression of cartilage degradation in the KLF5$^{+/-}$ limb was initiated around E16.5 (Fig. 2 and supplemental Fig. 2), these time courses support the hypothesis that MMP9 induction by KLF5 may lead to the cartilage degradation during endochondral ossification in skeletal development.

Since MMP9 is known to be strongly expressed in osteoclastic cells (26) and to play an important role in skeletal remodeling (3), we next investigated the effects of KLF5 on the culture of osteoclast precursor M-BMMΦ by retroviral overexpression of KLF5. Neither the osteoclastogenesis nor the MMP9 mRNA level was affected by the overexpression (Fig. 3, *D* and *E*). In the monocyte-macrophagic Raw264.7 cell culture as well, the adenoviral overexpression of KLF5 did not affect endogenous MMP9 mRNA level (supplemental Fig. 4*A*), whereas it increased the activity of the exogenously transfected luciferase reporter construct containing the MMP9 promoter above (supplemental Fig. 4*B*). These findings indicate that KLF5 does not have an important physiological function in osteoclastic cells.

To further examine the effect of loss of function of KLF5 in chondrocytes, we cultured primary costal chondrocytes derived from KLF5$^{+/-}$ mice and confirmed that the KLF5 mRNA level was decreased to about half that of wild-type chondrocytes (Fig. 4*A*). Among the molecules related to terminal differentiation of chondrocytes, cartilage degradation, and remodeling, only MMP9, and not osteopontin, MMP13, or VEGFA, was significantly suppressed by the KLF5 haploinsufficiency. Proliferative ability was comparable between cultured chondrocytes from KLF5$^{+/-}$ and the wild-type littermates (Fig. 4*B*). Gene silencing of KLF5 by RNA interference also caused the reduction of MMP9 mRNA expression in OUMS27 cells (Fig. 4*C*).

Finally, an immunohistochemical staining confirmed that MMP9 expression seen in the cartilage layer and the perichondrium of wild-type limb was scarcely detected in KLF5$^{+/-}$ (Fig. 4*D*). In the cartilage layer, the decreased MMP9 expression was correlated with the suppression of COL2 degradation and chondrocyte calcification, determined by immunohistochemical and von Kossa stainings, respectively. In the perichondrium, the MMP decrease was correlated with the suppression of DIPEN, which is a neoepitope at the aggrecan cleavage site generated by MMPs, and with that of CD34, which is an endothelial antigen representing blood vessels, determined by respective

immunostainings. Quantitative analyses actually revealed significant decreases in the width of the von Kossa-positive calcified layer and the number of CD34-positive blood vessels in the KLF5$^{+/-}$ limb (Fig. 4*E*).

DISCUSSION

The present *in vivo* analyses revealed that KLF5 haploinsufficiency caused impairment of cartilage matrix degradation and the subsequent remodeling to bone tissue, without affecting chondrocyte proliferation or differentiation. Microarray and cell culture analyses demonstrated that KLF5 contributes to the cartilage degradation through transcriptional induction of MMP9. MMP9 is known to be a potent proteinase that degrades denatured collagens and activates other MMPs and cytokines (4, 8, 27). In fact, the homozygous deficient mice (MMP9$^{-/-}$ mice) are reported to exhibit skeletal abnormality similar to KLF5$^{+/-}$ mice: elongation of hypertrophic layer, impaired vascularization, and delayed formation of bone and bone marrow cavity in the limbs (3), indicating a role of the KLF5-MMP9 axis during skeletal development.

It is, however, of note that the defect of KLF5 is physiologically more critical than that of MMP9, since KLF5$^{-/-}$ mice die *in utero* before E8.5, whereas MMP9$^{-/-}$ mice grow normally after birth, and MMP9$^{+/-}$ mice show no abnormality from embryos (3). This might be because KLF5 regulates molecules other than MMP9, since the present microarray analyses revealed up-regulation of several molecules like α-E-catenin (CTNNA1), ADAMTS4 (a disintegrin and metalloproteinase with thrombospondin-like repeat 4), interleukin-1, and MMP14 by the KLF5 overexpression in chondrogenic cells (Table 1 and supplemental Tables 1 and 2). α-E-catenin, a prototypic member of the α-catenin family and a component of the cadherin-catenin complex (28), is known to be required to sustain adhesion between cells during mammalian morphogenetic events (29). Although it is mainly expressed in epithelial tissues and the loss-of-function mutation causes human squamous cell carcinoma of the skin (30), the involvement in matrix degradation or angiogenesis remains unknown. Meanwhile, ADAMTS4 is a principal proteinase for aggrecan (31), a major cartilage matrix component that is degraded before collagenases cleave collagens in the hypertrophic layer (32). Hence, KLF5 might possibly lead to aggrecan degradation through induction of ADAMTS4, which is followed by matrix degradation by MMP9 (5). Interleukin-1, a representative proinflammatory cytokine, is also known to be a potent stimulator of MMPs, ADAMTSs, and other catabolic cytokines (32), so that interleukin-1 and MMP9 induced by KLF5 might initiate the subsequent catabolic changes of the cartilage. MMP14, although the induction by KLF5 was not strong (Table 1), is also a key proteinase in growth plate resorption, since the MMP-14-deficient mice exhibited dwarfism due to impaired endochondral ossification and angiogenesis, similarly to the KLF5$^{-/-}$ mice (33, 34). KLF5 may therefore be a crucial transcription factor that controls the molecular network for cartilage matrix degradation during endochondral ossification.

Another difference in the effects of insufficiency of KLF5 and MMP9 is their function in osteoclasts or chondroclasts. MMP9$^{-/-}$ mice showed abnormal bone remodeling after birth with impaired osteoclast recruitment, whereas KLF5$^{+/-}$ mice showed normal bone remodeling. Expression of MMP9 by osteoclastic cells may physiologically be important for skeletal development, since transplantation of wild-type bone marrow cells, including osteoclast progenitors, rescues the skeletal phenotype (3). In fact, MMP9 is abundantly expressed (26), whereas KLF5 was barely detected in osteoclastic cells (Fig. 1). The finding that the KLF5 overexpression in osteoclast precursors failed to alter endogenous MMP9 expression and osteoclastic differentiation (Fig. 3, *D* and *E*, and supplemental Fig. 4) supports the importance of MMP9 expression in osteoclastic cells. The present study, however, demonstrated that other than in osteoclasts, MMP9 was expressed in chondrocytes and perichondrium during skeletal development and was dramatically decreased by the KLF5 haploinsufficiency (Fig. 4*D*). This decrease was correlated with the suppression of COL2 degradation and an aggrecan cleavage neoepitope DIPEN. In addition, the induced MMP9 in chondrocytes by the KLF5 overexpression exerted a potent enzyme activity by gelatin zymography (Fig. 3*A*), as previously reported (35). These indicate a significant role of cell-autonomous action of MMP9 in chondrocytes in the process of cartilage degradation.

For endochondral ossification of hypertrophic chondrocytes, chondrocyte apoptosis, cartilage matrix degradation, and vascularization are tightly coupled (2, 5); however, which of these steps is rate-limiting remains unclear. A recent study on knockout mice of an antiapoptotic protein, galectin 3, has shown that acceleration of chondrocyte apoptosis was not associated with endochondral ossification (36), suggesting that chondrocyte apoptosis might be dispensable for the process. Several reports have indicated the matrix degradation and vascularization as the crucial steps (3, 5, 37–39), and, in fact, the present *in vivo* analyses showed that suppressions of MMP9 expression and cartilage matrix degradation by KLF5 insufficiency led to impairment of skeletal development accompanied by decreased vascularization (Fig. 4*D*). *In vitro* cultures, however, showed that a principal angiogenic factor, VEGFA (37–40), was little influenced by gain or loss of function of KLF5 in chondrocytes (Figs. 3*B* and 4*A*); nor were other angiogenic factors, VEGFC, VEGFD (41), HGF (42), FGF1, or FGF2 (43, 44), in the microarray analyses (supplemental Table 2). Hence, KLF5 is likely to regulate vascularization indirectly as a secondary effect of MMP9 secretion and matrix degradation in the cartilage layer and perichondrium, although the details need to be further investigated. In fact, cartilage explants from MMP9$^{-/-}$ mice in culture are reported to show a delayed angiogenesis (3). A previous report on MMP13$^{-/-}$ and MMP9$^{-/-}$ mice also showed that the cartilage matrix degradation was decreased in parallel with the pace that vasculature recruitment maintains with the slower rate of endochondral ossification (5). This evidence suggests that the matrix degradation may create a permissive environment for blood vessels to invade or make angiogenic factors accessible, leading to a hypothesis that cartilage degradation is a rate-limiting step for endochondral ossification of hypertrophic chondrocytes.

The skeletal abnormality of KLF5+/− mice was limited to the perinatal period and disappeared as the animals grew up after birth under physiological conditions. This may be due

to compensatory mechanisms for endochondral ossification, such as an increase of proteinases other than MMP9. In fact, proteinases, such as MMP13, tended to be regulated oppositely to MMP9 by the KLF5 overexpression (Fig. 3*B* and Table 1). Since MMPs are known to play roles under various pathological conditions, including wound healing, arthritis, and tumor development (45–47), we examined the effects of KLF5 insufficiency on bone fracture and arthritis by making the models in KLF5$^{+/-}$ mice at 8 weeks of age (supplemental Fig. 5, *A* and *B*). In results, there was no difference in fracture healing or arthritis development between KLF5$^{+/-}$ and the wild-type littermates. KLF5 may therefore be indispensable for skeletal development only in the perinatal period but be dispensable after birth under physiological and pathological conditions. Another possible compensatory mechanism is bone formation by osteoblasts, despite the expression of KLF5 in the cells (Fig. 1). This osteoblastic compensation may be sufficient to make up for the KLF5 dysfunction in chondrocytes after a substantial number of osteoblasts have appeared after birth but insufficient in the perinatal period when chondrocytes play central roles in endochondral ossification. Generation and evaluation of conditional knockout mice will clarify the tissue-specific roles of KLF5. In addition, further understanding of the molecular network related to the KLF5-MMP9 axis will greatly help us to unravel the complex mechanism modulating endochondral ossification.

REFERENCES

1. Kronenberg, H. M. (2003) *Nature* **423,** 332–336
2. Karsenty, G., and Wagner, E. F. (2002) *Dev. Cell* **2,** 389–406
3. Vu, T. H., Shipley, J. M., Bergers, G., Berger, J. E., Helms, J. A., Hanahan, D., Shapiro, S. D., Senior, R. M., and Werb, Z. (1998) *Cell* **93,** 411–422
4. Ortega, N., Behonick, D., Stickens, D., and Werb, Z. (2003) *Ann. N. Y. Acad. Sci.* **995,** 109–116
5. Stickens, D., Behonick, D. J., Ortega, N., Heyer, B., Hartenstein, B., Yu, Y., Fosang, A. J., Schorpp-Kistner, M., Angel, P., and Werb, Z. (2004) *Development* **131,** 5883–5895
6. Inada, M., Wang, Y., Byrne, M. H., Rahman, M. U., Miyaura, C., Lopez-Otin, C., and Krane, S. M. (2004) *Proc. Natl. Acad. Sci. U. S. A.* **101,** 17192–17197
7. Lee, E. R., Murphy, G., El-Alfy, M., Davoli, M. A., Lamplugh, L., Docherty, A. J., and Leblond, C. P. (1999) *Dev. Dyn.* **215,** 190–205
8. Werb, Z. (1997) *Cell* **91,** 439–442
9. Kaczynski, J., Cook, T., and Urrutia, R. (2003) *Genome Biol.* **4,** 206
10. van Vliet, J., Crofts, L. A., Quinlan, K. G., Czolij, R., Perkins, A. C., and Crossley, M. (2006) *Genomics* **87,** 474–482
11. Bieker, J. J. (2001) *J. Biol. Chem.* **276,** 34355–34358
12. Watanabe, N., Kurabayashi, M., Shimomura, Y., Kawai-Kowase, K., Hoshino, Y., Manabe, I., Watanabe, M., Aikawa, M., Kuro-o, M., Suzuki, T., Yazaki, Y., and Nagai, R. (1999) *Circ. Res.* **85,** 182–191
13. Ohnishi, S., Laub, F., Matsumoto, N., Asaka, M., Ramirez, F., Yoshida, T., and Terada, M. (2000) *Dev. Dyn.* **217,** 421–429
14. Conkright, M. D., Wani, M. A., Anderson, K. P., and Lingrel, J. B (1999) *Nucleic Acids Res.* **27,** 1263–1270
15. Shindo, T., Manabe, I., Fukushima, Y., Tobe, K., Aizawa, K., Miyamoto, S., Kawai-Kowase, K., Moriyama, N., Imai, Y., Kawakami, H., Nishimatsu, H., Ishikawa, T., Suzuki, T., Morita, H., Maemura, K., Sata, M., Hirata, Y., Komukai, M., Kagechika, H., Kadowaki, T., Kurabayashi, M., and Nagai, R. (2002) *Nat. Med.* **8,** 856–863
16. Oishi, Y., Manabe, I., Tobe, K., Tsushima, K., Shindo, T., Fujiu, K., Nishimura, G., Maemura, K., Yamauchi, T., Kubota, N., Suzuki, R., Kitamura, T., Akira, S., Kadowaki, T., and Nagai, R. (2005) *Cell Metab.* **1,** 27–39
17. Gollner, H., Dani, C., Phillips, B., Philipsen, S., and Suske, G. (2001) *Mech. Dev.* **106,** 77–83
18. Nakashima, K., Zhou, X., Kunkel, G., Zhang, Z., Deng, J. M., Behringer, R. R., and de Crombrugghe, B. (2002) *Cell* **108,** 17–29
19. Lefebvre, V., Garofalo, S., Zhou, G., Metsaranta, M., Vuorio, E., and De Crombrugghe, B. (1994) *Matrix Biol.* **14,** 329–335
20. Kobayashi, K., Takahashi, N., Jimi, E., Udagawa, N., Takami, M., Kotake, S., Nakagawa, N., Kinosaki, M., Yamaguchi, K., Shima, N., Yasuda, H., Morinaga, T., Higashio, K., Martin, T. J., and Suda, T. (2000) *J. Exp. Med.* **191,** 275–286
21. Aizawa, K., Suzuki, T., Kada, N., Ishihara, A., Kawai-Kowase, K., Matsumura, T., Sasaki, K., Munemasa, Y., Manabe, I., Kurabayashi, M., Collins, T., and Nagai, R. (2004) *J. Biol. Chem.* **279,** 70–76
22. Shimoaka, T., Kamekura, S., Chikuda, H., Hoshi, K., Chung, U. I., Akune, T., Maruyama, Z., Komori, T., Matsumoto, M., Ogawa, W., Terauchi, Y., Kadowaki, T., Nakamura, K., and Kawaguchi, H. (2004) *J. Biol. Chem.* **279,** 15314–15322
23. Yamada, T., Kawano, H., Koshizuka, Y., Fukuda, T., Yoshimura, K., Kamekura, S., Saito, T., Ikeda, T., Kawasaki, Y., Azuma, Y., Ikegawa, S., Hoshi, K., Chung, U. I., Nakamura, K., Kato, S., and Kawaguchi, H. (2006) *Nat. Med.* **12,** 665–670
24. Terato, K., Harper, D. S., Griffiths, M. M., Hasty, D. L., Ye, X. J., Cremer, M. A., and Seyer, J. M. (1995) *Autoimmunity* **22,** 137–147
25. Terato, K., Hasty, K. A., Reife, R. A., Cremer, M. A., Kang, A. H., and Stuart, J. M. (1992) *J. Immunol.* **148,** 2103–2108
26. Reponen, P., Sahlberg, C., Munaut, C., Thesleff, I., and Tryggvason, K. (1994) *Ann. N. Y. Acad. Sci.* **732,** 472–475
27. Engsig, M. T., Chen, Q. J., Vu, T. H., Pedersen, A. C., Therkidsen, B., Lund, L. R., Henriksen, K., Lenhard, T., Foged, N. T., Werb, Z., and Delaisse, J. M. (2000) *J. Cell Biol.* **151,** 879–889
28. Perez-Moreno, M., and Fuchs, E. (2006) *Dev. Cell* **11,** 601–612
29. Torres, M., Stoykova, A., Huber, O., Chowdhury, K., Bonaldo, P., Mansouri, A., Butz, S., Kemler, R., and Gruss, P. (1997) *Proc. Natl. Acad. Sci. U. S. A.* **94,** 901–906
30. Kobielak, A., and Fuchs, E. (2006) *Proc. Natl. Acad. Sci. U. S. A.* **103,** 2322–2327
31. Tortorella, M. D., Burn, T. C., Pratta, M. A., Abbaszade, I., Hollis, J. M., Liu, R., Rosenfeld, S. A., Copeland, R. A., Decicco, C. P., Wynn, R., Rockwell, A., Yang, F., Duke, J. L., Solomon, K., George, H., Bruckner, R., Nagase, H., Itoh, Y., Ellis, D. M., Ross, H., Wiswall, B. H., Murphy, K., Hillman, M. C., Jr., Hollis, G. F., Newton, R. C., Magolda, R. L., Trzaskos, J. M., and Arner, E. C. (1999) *Science* **284,** 1664–1666
32. Pratta, M. A., Yao, W., Decicco, C., Tortorella, M. D., Liu, R. Q., Copeland, R. A., Magolda, R., Newton, R. C., Trzaskos, J. M., and Arner, E. C. (2003) *J. Biol. Chem.* **278,** 45539–45545
33. Holmbeck, K., Bianco, P., Caterina, J., Yamada, S., Kromer, M., Kuznetsov, S. A., Mankani, M., Robey, P. G., Poole, A. R., Pidoux, I., Ward, J. M., and Birkedal-Hansen, H. (1999) *Cell* **99,** 81–92
34. Zhou, Z., Apte, S. S., Soininen, R., Cao, R., Baaklini, G. Y., Rauser, R. W., Wang, J., Cao, Y., and Tryggvason, K. (2000) *Proc. Natl. Acad. Sci. U. S. A.* **97,** 4052–4057
35. Haeusler, G., Walter, I., Helmreich, M., and Egerbacher, M. (2005) *Calcif. Tissue Int.* **76,** 326–335
36. Colnot, C., Sidhu, S. S., Balmain, N., and Poirier, F. (2001) *Dev. Biol.* **229,** 203–214
37. Gerber, H. P., Vu, T. H., Ryan, A. M., Kowalski, J., Werb, Z., and Ferrara, N. (1999) *Nat. Med.* **5,** 623–628
38. Maes, C., Carmeliet, P., Moermans, K., Stockmans, I., Smets, N., Collen, D., Bouillon, R., and Carmeliet, G. (2002) *Mech. Dev.* **111,** 61–73
39. Zelzer, E., Mamluk, R., Ferrara, N., Johnson, R. S., Schipani, E., and Olsen, B. R. (2004) *Development* **131,** 2161–2171
40. Zelzer, E., McLean, W., Ng, Y. S., Fukai, N., Reginato, A. M., Lovejoy, S., D'Amore, P. A., and Olsen, B. R. (2002) *Development* **129,** 1893–1904
41. Bluteau, G., Julien, M., Magne, D., Mallein-Gerin, F., Weiss, P., Daculsi, G., and Guicheux, J. (2007) *Bone* **40,** 568–576
42. Naldini, L., Vigna, E., Bardelli, A., Follenzi, A., Galimi, F., and Comoglio, P. M. (1995) *J. Biol. Chem.* **270,** 603–611

43. Jingushi, S., Scully, S. P., Joyce, M. E., Sugioka, Y., and Bolander, M. E. (1995) *J. Orthop. Res.* **13,** 761–768
44. Whitelock, J. M., Murdoch, A. D., Iozzo, R. V., and Underwood, P. A. (1996) *J. Biol. Chem.* **271,** 10079–10086
45. Milner, J. M., and Cawston, T. E. (2005) *Curr. Drug Targets Inflamm. Allergy* **4,** 363–375
46. Colnot, C., Thompson, Z., Miclau, T., Werb, Z., and Helms, J. A. (2003) *Development* **130,** 4123–4133
47. Kosaki, N., Takaishi, H., Kamekura, S., Kimura, T., Okada, Y., Minqi, L., Amizuka, N., Chung, U. I., Nakamura, K., Kawaguchi, H., Toyama, Y., and D'Armiento, J. (2007) *Biochem. Biophys. Res. Commun.* **354,** 846–851

Osteoarthritis and Cartilage (2008) **16,** 1300–1306

doi:10.1016/j.joca.2008.03.011

Osteoarthritis and Cartilage

International Cartilage Repair Society

OARSI OSTEOARTHRITIS RESEARCH SOCIETY INTERNATIONAL

Fully automatic quantification of knee osteoarthritis severity on plain radiographs

H. Oka M.D.†, S. Muraki M.D., Ph.D.†, T. Akune M.D., Ph.D.†, A. Mabuchi M.D., Ph.D.†, T. Suzuki M.D., Ph.D.‡, H. Yoshida M.D., Ph.D.‡, S. Yamamoto M.D., Ph.D.‡, K. Nakamura M.D., Ph.D.§, N. Yoshimura M.D., Ph.D.† and H. Kawaguchi M.D., Ph.D.§*

† *22nd Century Medical Center, The University of Tokyo, Tokyo, Japan*

‡ *Tokyo Metropolitan Institute of Gerontology, Tokyo, Japan*

§ *Sensory and Motor System Medicine, The University of Tokyo, Tokyo, Japan*

Summary

Objective: Although knee osteoarthritis (OA) is a major public health issue causing chronic disability, there is no objective or accurate method for measurement of the structural severity in general clinical practice. Here we have established a fully automatic program KOACAD (knee OA computer-aided diagnosis) to quantify the major OA parameters on plain knee radiographs, validated the reproducibility and reliability, and investigated the association of the parameters with knee pain.

Methods: KOACAD was programmed to measure joint space narrowing at medial and lateral sides, osteophyte formation, and joint angulation. Anteroposterior radiographs of 1979 knees of a large-scale cohort population were analyzed by KOACAD and conventional categorical grading systems.

Results: KOACAD automatically measured all parameters in less than 1 s without intra- or interobserver variability. All parameters, especially medial joint space narrowing, were significantly correlated with the conventional gradings. In the parameters, osteophyte formation was associated with none of the joint space parameters, suggesting different etiologic mechanisms between them. Multivariate logistic regression analysis after adjustment for age and confounding factors revealed that medial joint space narrowing and varus angulation of knee joints were risk factors for the presence of pain (594/1979 knees), while neither lateral joint space nor osteophyte area was.

Conclusion: KOACAD was shown to be useful for objective, accurate, simple and easy evaluation of the radiographic knee OA severity in daily clinical practice. This system may also serve as a surrogate measure for the development of disease-modifying drugs for OA, just as bone mineral density does in osteoporosis.

Key words: Osteoarthritis, Knee, Diagnosis, Computer-aided diagnosis, Imaging, Plain radiograph.

Introduction

Due to the rapidly increasing fraction of aging people today, osteoarthritis (OA) is now considered as a major public health issue causing chronic disability in most developed countries. It is estimated that up to 10% of the entire world population, and more than 50% of those aged over 50 years, are suffering from OA[1]. Knee OA, affecting about 30% of those over 65 years and as often associated with disability as heart and chronic lung diseases[2,3], is characterized by pathological features including joint space narrowing, osteophyte formation, and joint angulation. Although OA and osteoporosis are the two major skeletal disorders with strong social impact[4], OA falls far behind osteoporosis in the assessment of its disease severity and in the development of disease-modifying drugs. This is mainly due to the lack of an objective and accurate method to evaluate the structural severity and thereby to assess the efficacy of drugs as surrogate measures like bone mineral density (BMD) in osteoporosis.

Although magnetic resonance imaging (MRI) with high resolution has been rapidly advanced as a promising technique, it is still too laborious and expensive to perform in general clinical practice or in population-based epidemiologic studies, and the interpretation remains controversial as a primary end-point in clinical trials of the disease-modifying drugs[5–7]. Biochemical markers of cartilage turnover are being tested to measure the disease progression; however, their validation as a surrogate measure will require significant additional work[5,8]. Hence, plain radiography is considered the gold standard as a method that is non-invasive, inexpensive, convenient, simple, and fast to use in assessing OA severity. The most conventional system to grade the radiographic severity has been the Kellgren/Lawrence (K/L) grading[9]. However, this categorical system is limited by incorrect assumptions that progression of distinct OA features like joint space narrowing and osteophyte formation is linear and constant, and that their relationships are proportional. Since the system emphasizes the development of osteophytes, it is unclear how to handle knees with severe joint space narrowing but no osteophyte formation. To overcome the problem,

*Address correspondence and reprint requests to: Dr Hiroshi Kawaguchi, M.D., Ph.D., Sensory and Motor System Medicine, Faculty of Medicine, The University of Tokyo, Hongo 7-3-1, Bunkyo, Tokyo 113-8655, Japan. Tel: 81-3-3815-5411 ext. 30473; Fax: 81-3-3818-4082; E-mail: kawaguchi-ort@h.u-tokyo.ac.jp

Received 3 January 2008; revision accepted 9 March 2008.

a radiographic atlas of individual features was published by the OA Research Society International (OARSI) in 1995[10] and a revised version in 2007[11]. This system separately evaluates joint space narrowing and osteophyte formation at the medial and lateral tibiofemoral compartments on radiographs; however, the grading is still limited in reproducibility and sensitivity due to the subjective judgment of individual observers and the categorical classification into four-grade (0–3) scales. Although several semi-automatic methods for objective measurement with continuous variables of joint space or angle using computer-assisted systems have recently been developed, there still remain intra- and interobserver variabilities since initial operations like identifying points or drawing lines must be manually performed[12–16].

The present study has developed a novel computer program, KOACAD (knee OA computer-aided diagnosis), which for the first time has realized a fully automatic measurement of major parameters of knee OA: joint space area (JSA) and the minimum joint space width (mJSW) at medial and lateral sides, osteophyte area, and tibiofemoral angle (TFA) on plain anteroposterior radiographs. We examined the reproducibility and reliability of KOACAD by comparing it with conventional grading systems and semi-automatic measurements.

Arthritis is the most common cause of pain in the elderly[17], and knee pain is the principal clinical symptom of knee OA. Although much effort has been devoted toward a definition of knee pain, the correlation with radiographic severity of the knee OA was not as strong as one would expect[18–20]. Hence, this study finally sought to identify radiographic factors related to knee pain by examining the association of the KOACAD parameters with the presence of pain using a baseline database of our large-scale OA cohort study ROAD (research on OA against disability).

Subjects and methods

SUBJECTS

The ROAD study is a nationwide OA cohort study that started in 2005, and is constituted of four cohorts. So far, we have completed creation of a baseline database including clinical and genomic information of 3040 participants in three cohorts in urban, mountainous, and seacoast areas. The database includes anteroposterior and lateral radiographs of bilateral knees of all participants. For evaluation of the KOACAD system, we used 1979 anteroposterior radiographs from 2002 knees of 1001 participants of the urban cohort after 15 artificial knee joints and eight knees with more than 5° flexion contracture were omitted. The study was conducted with approval of the Institutional Review Boards (IRBs) of the University of Tokyo and the Tokyo Metropolitan Institute of Gerontology, and all participants provided written informed consent.

RADIOGRAPHY

Plain radiographs with standing on both legs and the knee extended were taken with a horizontal X-ray beam unless otherwise described, using a Fuji 5000 Plus Reader on a 36 × 46 cm Fuji ST-VI Computed Radiography (CR) imaging plate (Fuji Medical Systems, Tokyo, Japan) with a 20 × 30 mm rectangular metal plate beside it as a magnification index. Rotation of the foot was adjusted to keep the second metatarsal bone parallel to the X-ray beam. Images were downloaded into Digital Imaging and Communication in Medicine (DICOM) format files with a spatial resolution of 1584 × 2016 pixels (giving a pixel size of 0.01 mm) and 1024 gray levels.

IMAGE PROCESSING BY KOACAD

The KOACAD was programmed to perform the following operations automatically on the digital images above using the object-oriented programming language C++ [Fig. 1(A)]. Initially, correction for radiographic magnification was performed based on the image size of the rectangular metal plate. To reduce the image noise, the entire radiograph underwent filtering three times with a 3 × 3 square neighborhood median filter as reported previously[21]. Then, the Robert's filter was applied to extract the rough outlines of tibia and femur, so that medial and lateral sides could be judged by the difference of calculated widths of tibia and fibula at the level of 100 pixels above the bottom of the image [Fig. 1(B)].

Next, to determine the region of interest (ROI) including the tibiofemoral joint space, a vertical neighborhood difference filter was applied to identify points with high absolute values of difference of scales. The center of all the points was then calculated, and 480 × 200 pixels of a rectangle with the center was decided as the ROI [Fig. 1(C)]. Within the ROI, the outline of femoral condyle was designated as the upper rim of the joint space by vertical filtering with the 3 × 3 square neighborhood difference filter [Fig. 1(D)]. The two ends were determined using a Canny's filter to remove the noise of lines[22], and vertical lines from the ends were designated as the outside rims of the joint space. Outlines of anterior and posterior margins of the tibial plateau were drawn similarly to that of the femoral condyle, and the middle line between the two outlines was designated as the lower rim of the joint space [Fig. 1(E)]. Then, a straight regression line for the lower rim outline was drawn, and their intersections were designated as the inside rims [Fig. 1(F)]. The medial and lateral JSAs were determined as the areas surrounded by the upper, lower, inside, and outside rims above [Fig. 1(G)]. The medial and lateral mJSWs were further determined as the minimum vertical distances in the respective JSA [Fig. 1(H)].

To measure osteophyte area and TFA, the medial and lateral outlines of femur and tibia were drawn by the 3 × 3 square horizontal neighborhood difference filter and Canny's filter as described above. Then, the inflection points for the outlines were calculated. The medial outline of the tibia from the inflection point was drawn upward to the joint level [Fig. 1(I)], and the area that was medially prominent over the smoothly extended outline was designated as the osteophyte area [Fig. 1(J)]. For TFA, a middle line between the medial and lateral outlines of the femur from the top of the image to the inflection points was drawn [Fig. 1(K)], and the straight regression line was determined to be the axis of the femur. Similarly, the straight regression line of the middle line of the tibia from the bottom to the inflection points was designated as the axis of the tibia. The lateral angle between the two axis lines was calculated as TFA [Fig. 1(L)].

ANALYSES

To decide the ideal conditions for the taking of radiographs for the KOACAD analysis, we initially evaluated the reproducibility of the six parameters by an intraclass coefficient of correlation (ICC) on radiographs of 20 individuals taken at a 2-week interval with various knee flexion angles (0, 10, 20, and 30°) and X-ray beam angulations (0, 5, 10, and 15°).

Conventional gradings by the K/L system and the OARSI radiographic atlas were performed by experienced orthopedists on 50 radiographs randomly selected from the 1979 radiographs above, and intra- and interobserver variabilities were evaluated by κ values. The KOACAD parameters were also evaluated by semi-automatic measurement by a conventional computer-assisted program (Quick Grain Standard, Inotech, Hiroshima, Japan) after drawing of the outlines of femur and tibia by the orthopedists, and intra- and interobserver ICCs of each parameter were compared with those of KOACAD.

Correlations of the KOACAD parameters with the K/L grading (0–4) were examined by Spearman's correlation test on the entire 1979 radiographs. Correlations with the OARSI grading (0–3) were similarly examined for five common parameters: the KOACAD mJSW and JSA at the medial and lateral sides were compared with the OARSI joint space narrowing grades at the respective sides, and the KOACAD osteophyte area with the OARSI osteophyte grade of the medial tibial plateau. Since there was no radiograph of OARSI grade 3 of lateral joint space narrowing, correlations of the KOACAD lateral JSA and lateral mJSW were examined with the OARSI grade 0–2.

Correlations among the KOACAD parameters were analyzed using Pearson's correlation test, and parameters with correlation value of more than 0.5 were defined as confounding factors.

For the assessment of factors associated with symptomatic knee pain, age and the six KOACAD parameters were compared between knees with and without pain by Student's t test on the 1979 radiographs. Logistic regression analyses were used to estimate odds ratio (OR) and the associated 95% confidence interval (CI). Final multivariate logistic models were created through stepwise elimination of variables of interest from univariate analysis after adjustment for age and confounding factors.

A P-value of <0.05 for analysis of safety variables was considered significant. Data analyses were performed using SAS version 9.0 (SAS Institute Inc., NC, USA).

Results

REPRODUCIBILITY OF KOACAD PARAMETERS BY KNEE FLEXION ANGLES AND X-RAY BEAM ANGULATIONS

The KOACAD system could automatically measure the six parameters on an anteroposterior knee radiograph in

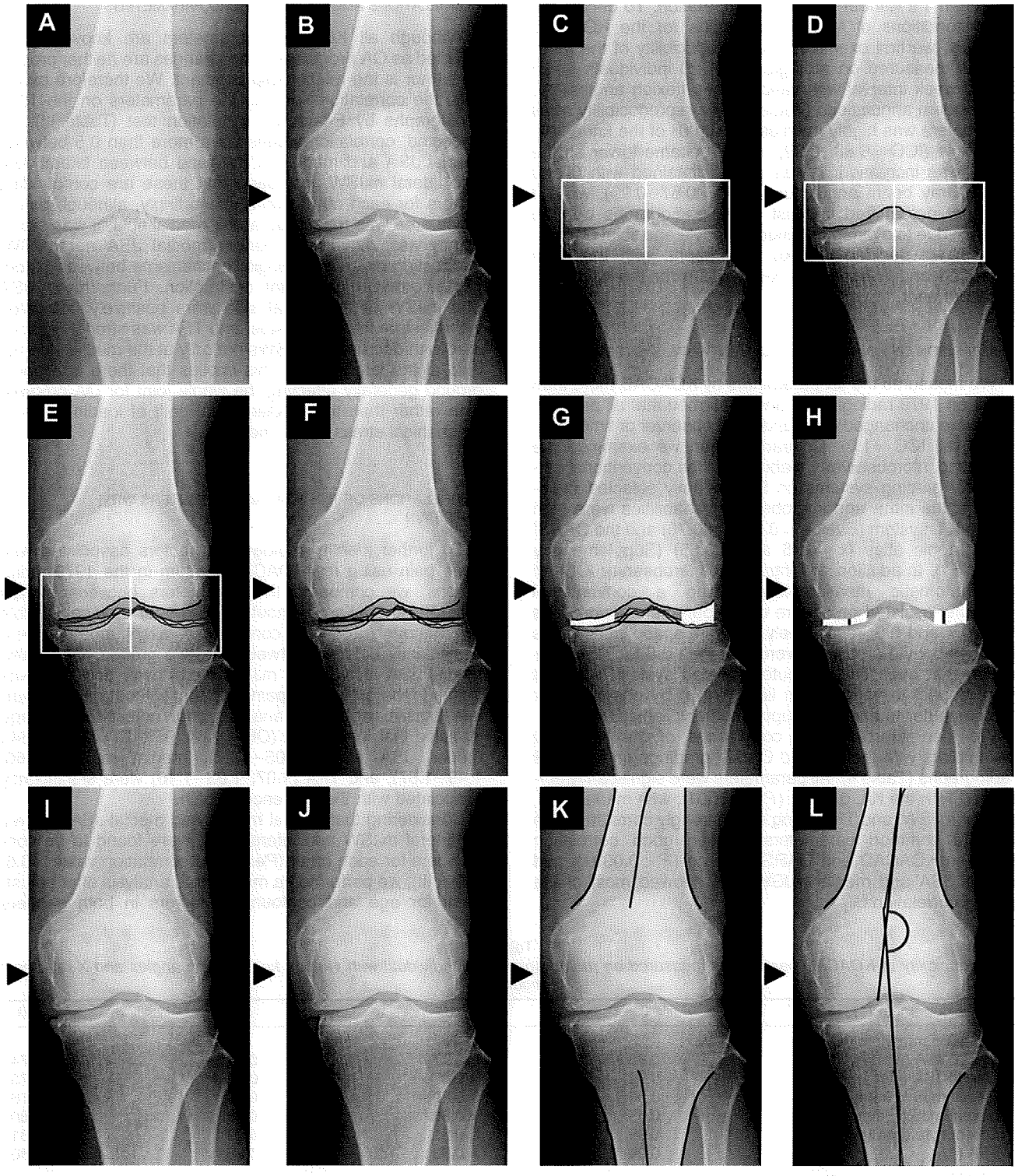

Fig. 1. Schema of image processing by KOACAD. (A) A digitized knee radiograph as a DICOM file. (B) Filterings to reduce the image noise and to extract outlines of tibia and femur. (C) ROI and the center including the tibiofemoral joint space. (D) An outline of femoral condyle (blue line) as the upper and outside rims of the joint space. (E) Outlines of anterior and posterior margins of the tibial plateau (green lines), and the middle line between the two outlines (red line) as the lower rim of the joint space. (F) A straight regression line (black line) for the lower rim line, and their intersections as the inside rims. (G) Medial and lateral JSAs (white areas) surrounded by the upper, lower, inside, and outside rims. (H) Medial and lateral mJSWs (brown lines) as the minimum vertical distances in the JSAs. (I) Medial outline (blue line) of the tibia drawn from the calculated inflection point upward to the joint level. (J) Osteophyte area (red area) that is medially prominent over the smoothly extended outline of the tibia. (K) Medial and lateral outlines (blue lines) of the femur and tibia from the edges of the image to the inflection points, and the middle lines (purple lines). (L) TFA as the lateral angle between the straight regression lines (black lines) of the middle lines above in the femur and tibia.

less than 1 s without any manual operation. To decide the ideal conditions of taking radiographs for the KOACAD analysis, we first examined the reproducibility of the parameters measured on radiographs of 20 individuals taken at a 2-week interval with various knee flexion angles and X-ray beam angulations (Table I). The reproducibility of all parameters was highly maintained with 0° of the knee flexion angle (ICC = 0.88–0.99), which became lower as the angle was increased. It was also maintained with 0 and 5° of X-ray beam angulations (ICC = 0.87–0.99), while it was not determined in most of the radiographs with 10 and 15° due to overlap of femoral condyle and tibial plateau. Hence, we decided to take radiographs with the knee extended and a horizontal X-ray beam for the KOACAD measurement.

COMPARISON OF KOACAD WITH CONVENTIONAL SYSTEMS

We measured the six parameters by KOACAD more than twice on 1979 radiographs, and confirmed that all parameters were unchanged independent of observer or time measured (all ICC = 1.0). Contrarily, when we examined the intra- and interobserver variabilities of the conventional categorical grading systems on 50 randomly selected radiographs, the intra- and interobserver variabilities were high by the K/L system (κ value = 0.84 and 0.76) and the OARSI radiographic atlas ($\kappa \leq 0.75$ and ≤ 0.65) (Supplementary Table S1). In addition, the intra- and interobserver ICCs of semi-automatic measurements using a conventional computer-assisted procedure of the parameters were less than 0.7 and 0.6, respectively, for joint space parameters and osteophyte area, and were less than 0.8 for TFA, indicating that even this computer-assisted system is robust with respect to variability in lines drawn by observers for the computer to analyze (Supplementary Table S1).

We then examined the correlations of the KOACAD parameters with the K/L and OARSI gradings on the 1979 radiographs (Table II). All parameters were significantly correlated with the K/L grading ($P < 0.0001$); with medial JSA, medial mJSW, and TFA being most strongly correlated with it. Five common parameters showed good correlation between KOACAD and OARSI grading ($P < 0.0001$), and medial JSA and medial mJSW also showed most of the strong correlations.

CORRELATIONS AMONG THE KOACAD PARAMETERS

Although all KOACAD parameters are known to be affected as OA progresses, the changes are neither proportional nor is the relationship constant. We therefore examined the correlations among the parameters on the 1979 radiographs by Pearson's correlation test (Table III). As expected, correlation values were more than 0.5 between medial JSA and medial mJSW, and between lateral JSA and lateral mJSW, indicating that these are confounding factors for each other. More interestingly, although osteophyte area was measured at the medial tibia, it was significantly associated with neither medial JSA nor mJSW, suggesting different etiologic mechanisms between osteophyte formation and joint destruction. Furthermore, JSA and mJSW at the lateral side were positively correlated with those at the medial side, and TFA was strongly associated with decreased mJSWs not only at the medial side but also at the lateral side. This implies that there is a background generally affecting the whole joint for OA progression rather than the medial-lateral shift of loading axis of mechanical stress within the joint.

CORRELATIONS OF THE KOACAD PARAMETERS WITH KNEE PAIN

To further identify radiographic factors associated with knee pain using the KOACAD system in the 1979 radiographs, we compared the parameters between groups with (594 knees) and without (1385 knees) knee pain (Table IV). Although age was comparable, all parameters were significantly different between the two groups. Especially, medial JSA and medial mJSW were lower and TFA was higher in the group with pain than that without pain. Univariate logistic regression analysis after adjustment for age revealed that female sex (OR = 1.64; 95% CI = 1.47–1.84), medial JSA (1.16; 1.05–1.27), medial mJSW (1.66; 1.49–1.87), and TFA (1.07; 1.03–1.10) were significantly associated with the presence of pain.

Considering that medial mJSW and medial JSA, as well as lateral mJSW and lateral JSA, were found to be confounders for each other (Pearson's correlation value > 0.5; Table III), we performed a multivariate analysis after adjustment for age and confounding factors in both genders

Table I

Reproducibility of KOACAD parameters measured on radiographs of an individual with various knee flexion angles and X-ray beam angulations

Knee flexion angle (°)	0	10	20	30
KOACAD parameters (ICC)				
Medial JSA (mm^2)	0.88	0.77	0.74	0.74
Lateral JSA (mm^2)	0.92	0.87	0.73	0.73
Medial mJSW (mm)	0.96	0.92	0.90	0.78
Lateral mJSW (mm)	0.95	0.86	0.88	0.80
Osteophyte area (mm^2)	0.99	0.91	0.79	0.81
TFA (°)	0.94	0.93	0.86	0.86
X-ray beam angulation (°)	0	5	10	15
KOACAD parameters (ICC)				
Medial JSA (mm^2)	0.88	0.87	ND	ND
Lateral JSA (mm^2)	0.92	0.92	(17/20)	(20/20)
Medial mJSW (mm)	0.96	0.96		
Lateral mJSW (mm)	0.95	0.95		
Osteophyte area (mm^2)	0.99	0.99		
TFA (°)	0.94	0.93		

Reproducibility of six parameters was evaluated by an ICC on radiographs of 20 individuals taken at a 2-week interval. ND: not determined due to overlap of femur and tibia.

Table II
Correlations of the KOACAD parameters with the K/L and OARSI gradings

	0	1	2	3	4	R^2
K/L grading						
Number	162	625	956	205	31	
Medial JSA (mm^2)	112.4 ± 1.8	97.0 ± 0.9	91.1 ± 0.7	83.2 ± 1.9	52.4 ± 5.4	−0.29
Lateral JSA (mm^2)	114.3 ± 2.0	110.6 ± 1.1	107.2 ± 0.9	105.3 ± 1.9	106.2 ± 6.1	−0.09
Medial mJSW (mm)	3.9 ± 0.1	3.4 ± 0.0	3.1 ± 0.0	2.5 ± 0.1	1.5 ± 0.2	−0.41
Lateral mJSW (mm)	4.7 ± 0.1	4.4 ± 0.0	4.3 ± 0.1	4.2 ± 0.1	4.2 ± 0.3	−0.11
Osteophyte area (mm^2)	2.7 ± 1.4	2.0 ± 0.2	3.2 ± 0.2	7.9 ± 1.3	10.9 ± 4.2	0.15
TFA (°)	175.7 ± 0.2	176.2 ± 0.1	177.4 ± 0.1	179.6 ± 0.3	184.2 ± 1.2	0.31
OARSI grading						
Medial JSA (mm^2) (n)	105.9 ± 0.9 (602)	89.8 ± 0.7 (953)	90.0 ± 1.3 (317)	65.4 ± 2.2 (107)		−0.34
Lateral JSA (mm^2) (n)	109.6 ± 0.6 (1926)	87.7 ± 4.2 (38)	61.7 ± 7.3 (15)	− (0)		−0.16
Medial mJSW (mm) (n)	3.6 ± 0.0 (602)	3.1 ± 0.0 (953)	2.7 ± 0.0 (317)	1.8 ± 0.1 (107)		−0.45
Lateral mJSW (mm) (n)	4.3 ± 0.0 (1926)	3.3 ± 0.2 (38)	2.5 ± 0.3 (15)	− (0)		−0.19
Osteophyte area (mm^2) (n)	2.0 ± 0.2 (1212)	2.8 ± 0.4 (421)	4.7 ± 0.6 (215)	14.7 ± 0.7 (131)		0.25

Analyses were performed by Spearman's correlation test on 1979 radiographs, and data are expressed by means ± S.E.M. (all *P*-values < 0.0001).

(Table V). It was found that low medial mJSW and high TFA were associated with the presence of pain, while neither lateral mJSW nor osteophyte area was.

Discussion

In the present study, we established a fully automatic computer-assisted program, KOACAD that can quantitate the major features of knee OA on plain radiographs. This system has achieved objective, accurate, simple and easy assessment of the structural severity of knee OA without any manual operation in general clinical practice or in population-based epidemiologic studies. The system could also accurately evaluate distinct features of knee OA like joint space narrowing, osteophyte formation, and joint angulation in one sitting. By applying this system to the baseline data in the ROAD study, medial joint space narrowing and varus angulation, though neither lateral joint space narrowing nor osteophyte formation, was shown to be associated with symptomatic knee pain.

Independent measurement of the parameters by KOACAD enabled us to examine the correlation of distinct features of OA, which may lead to better understanding of the OA pathophysiology. For example, a lack of association between osteophyte formation and joint space narrowing indicates independent backgrounds of the two representative features of knee OA. A previous prospective study using a famous OA cohort, the Chingford study, has reported that there was no association between the two features[23]. Although the authors described in the paper that this might possibly be due to inaccurate and subjective measurement on radiographs, the present KOACAD analysis has confirmed the reliability by accurate and objective measurement. A recent cross-sectional study has also shown that osteophyte formation was unrelated not only to joint space narrowing on plain radiographs, but also to cartilage loss measured by quantitative MRI[24]. Furthermore, by creating an OA model through induction of instability in mouse knee joints, we have identified a cartilage specific molecule, carminerin, that regulates osteophyte formation without affecting cartilage destruction during the OA progression[25,26]. Further clinical and basic research will disclose the distinct backgrounds of the two OA features. The correlation analysis among the parameters also revealed that joint space narrowing at medial and lateral sides was positively correlated, indicating an etiologic mechanism that affects the whole joint. Although this does not necessarily deny the mechanistic contribution of medial-lateral shift of the loading axis within the joint to the OA progression, the limitation of efficacy of a valgus knee brace, lateral wedged insole, or valgus high tibial osteotomy for medial compartment OA of the knee may at least partly be explained by the result.

For accurate and reproducible assessment of tibiofemoral joint space on plain radiographs, a variety of radiographic methods have been developed. Several reports have claimed that positioning of the knee with several angles of flexion provides more accurate joint space measurement than conventional extended knees due to superimposition of the anterior and posterior margins of the tibial plateau[13,27,28]. Among the reports, angulation of the X-ray beam and rotation of the foot were different, and some of them included fluoroscopic assistance for the adjustment of margins of the tibial plateau. Despite these efforts, none of the radiographic protocols has realized high reproducibility or sensitivity for long-term longitudinal

Table III
Correlations among the KOACAD parameters

	Medial JSA	Lateral JSA	Medial mJSW	Lateral mJSW	Osteopyte area	TFA
Medial JSA	1.00					
Lateral JSA	0.22 (<0.0001)	1.00				
Medial mJSW	0.70 (<0.0001)	0.13 (0.0008)	1.00			
Lateral mJSW	0.18 (<0.0001)	0.72 (<0.0001)	0.22 (<0.0001)	1.00		
Osteophyte area	0.02 (NS)	−0.13 (0.0006)	0.04 (NS)	−0.13 (NS)	1.00	
TFA	−0.08 (0.03)	0.03 (NS)	−0.21 (<0.0001)	−0.19 (<0.0001)	−0.02 (NS)	1.00

Analyses were performed by Pearson's correlation test on 1979 radiographs, and data are expressed as Pearson's correlation values and *P*-values in the parentheses. NS: not significant ($P > 0.05$).

Table IV
Differences of age and the KOACAD parameters between knees with and without pain

	Pain (+)	Pain (−)	*P*-value
Participants (men/women)	594 (124/470)	1385 (575/810)	
Age (years)	76.8 ± 4.7	77.0 ± 4.4	NS
Parameters			
Medial JSA (mm^2)	88.0 ± 1.0	95.7 ± 0.7	<0.0001
Lateral JSA (mm^2)	105.9 ± 1.1	110.2 ± 0.7	0.0013
Medial mJSW (mm)	2.9 ± 1.0	3.3 ± 1.2	<0.0001
Lateral mJSW (mm)	4.3 ± 0.1	4.4 ± 0.0	0.0044
Osteophyte area (mm^2)	4.8 ± 5.4	2.9 ± 7.0	0.0002
TFA (°)	177.9 ± 3.3	176.9 ± 4.3	<0.0001

Analyses were performed on 1979 radiographs, and data are expressed by means ± S.E.M. *P*-values were determined by Student's *t* test. NS: not significant ($P > 0.05$).

studies[27,29]. And, first of all, since these methods increase the cost and require the technician to be specifically trained, they are unlikely to be applicable in general clinical practice or population-based epidemiologic studies. Meanwhile, the conventional standing extended view knee radiographs that the KOACAD system adopted are known to be sensitive to change if the tibial plateau is adequately aligned[30]. To overcome variability of the tibiofemoral joint space by the positioning of the knee and the angulation of the X-ray beam causing the misalignment of the anterior and posterior margins of the tibial plateau, the KOACAD system for the first time designated the middle line between outlines of anterior and posterior margins of the tibial plateau as the lower rim of the radiographic joint space. In fact, reproducibility of all KOACAD parameters was highly maintained with 0° knee flexion and 0–5° X-ray angulation (Table I). This, however, indicates that OA patients with flexion contracture of the knee cannot be appropriately assessed by the KOACAD system, so that patients with more than 5° flexion contracture were excluded from the present study.

Digital images by computed radiographic techniques offer several advantages compared with conventional analog film-screen radiography, and are increasingly available in routine patient management because they allow image enhancement, quantification, archiving, transmission, simultaneous access to the image at multiple sites, and reduction in radiation dose[31]. Although this study used digitized images as the DICOM file, we have confirmed that images digitized from analog radiographs by general image scanners could be used for the KOACAD analysis with perfect reproducibility (ICC = 1.0). In addition, since KOACAD is programmed based on a personal computer, and not on a massive workstation, it can be used anywhere, even away from clinics.

Table V
Multivariate logistic regression analysis for OR and 95% CI of the KOACAD parameters for knee pain

	Men (699)		Women (1280)	
	OR	95% CI	OR	95% CI
Medial mJSW	1.46	1.16–1.90	1.41	1.23–1.63
Lateral mJSW	0.99	0.79–1.23	1.10	0.98–1.24
Osteophyte area	0.99	0.96–1.04	0.99	0.98–1.00
TFA	1.07	1.01–1.13	1.07	1.03–1.10

Data were calculated by stepwise logistic regression analysis after adjustment for age and confounding factors on 1979 radiographs.

The relationship between the radiographic findings and the symptomatic pain in knee joints remains controversial, but at least the severity of radiographic OA is not linearly correlated with that of pain[18–20]. Although the present multivariate analysis was able to detect significant associations of knee pain with low medial mJSW and high TFA, they were not strong (Table V). This may be due to the complicated mechanism underlying the pain. Although articular cartilage is viewed as a major target tissue of OA, knee pain may arise from a number of different structures like joint capsule, ligaments, menisci, bursae, and the bone marrow. Pathological structures caused by OA may contribute to pain indirectly. For example, inflammatory synovitis and associated capillaries are innervated by pain fibers and may be affected in OA[32]. Furthermore, previous MRI surveys among patients with radiographic knee OA showed that knee pain was due not only to OA-related disorders, but also to spontaneous osteonecrosis and bone marrow edema around the knee joint[33–35]. A limitation of the KOACAD system is that these periarticular disorders are not included in the parameters but are best shown by MRI, which might possibly lead to failures in the treatment of knee pain.

Another limitation of this study is a lack of longitudinal investigation to validate the sensitivity of the KOACAD system. One criticism has been that plain radiographs are insensitive to change over time, and that even a small radiographic change is associated with substantial cartilage loss[36]. Nevertheless, the current recommendations suggest that clinical studies of knee OA should include a structural measure of OA severity[5,28]. This emphasizes the need for further refinement in the definition of radiographic outcomes in prospective clinical trials. Recent longitudinal studies using quantitative MRI have shown that subjects with knee OA lose 5% of their tibial cartilage volume per year[37,38] and that the cartilage loss is correlated with worsening of symptoms and portends knee replacement[20,39]. Although the cartilage loss detected by quantitative MRI is much greater than that detected in plain radiographs, the MRI-based cartilage volume correlates with the change of radiographic features to some extent[40,41]. Since the KOACAD system can provide continuous measures of parameters of OA severity, it is possible that the system is as sensitive to change over time as quantitative MRI. Also, the association between knee pain and radiographic features cannot be appropriately assessed in a cross-sectional survey, but should be evaluated over a defined period of time, as indicated by previous reports[42,43]. Our baseline survey in the ROAD study has included quantitative MRI on a group of randomly selected participants. In 2008–2010, we are planning a second survey including the KOACAD radiographic analysis on more than 3000 participants and the quantitative MRI on a portion of these. Comparison of the KOACAD parameters and the MRI findings will validate the sensitivity of the KOACAD system over time, and lead to further understanding of the association between knee pain and radiographic features.

In conclusion, we have established a fully automatic computer-assisted program, KOACAD, to quantify knee OA severity on plain radiographs, and validated its high reproducibility and reliability in a cross-sectional study. This system may not only be useful for objective evaluation of knee OA patients in daily clinical practice or in population-based epidemiologic studies, but also act as a proper surrogate measure for the development of disease-modifying drugs for OA. We hope in the future that this system will be prevalently used worldwide to lead to international criteria for diagnosis and treatment of knee OA, just like BMD in osteoporosis.

Conflict of interest

There are no conflicts of interest.

Acknowledgments

This work was supported by a Grant-in-Aid for Young Scientists from the Japanese Ministry of Education, Culture, Sports, Science and Technology (A18689031), H17-Men-eki-009 from the Ministry of Health, Labor and Welfare, and Research Aid from the Japanese Orthopaedic Association.

Supplementary material

Supplementary material for this article may be found, in the online version, at doi: 10.1016/j.joca.2008.03.011.

References

1. Sharma L, Kapoor D. Epidemiology of osteoarthritis. In: Moskowitz RW, Altman RD, Hochberg MC, Buckwalter JA, Goldberg VM, Eds. Osteoarthritis: Diagnosis and Medical/Surgical Management. 4th edn. Philadelphia: Lippincott Williams & Wilkins; 2007:3–26.
2. Guccione AA, Felson DT, Anderson JJ, Anthony JM, Zhang Y, Wilson PW, *et al.* The effects of specific medical conditions on the functional limitations of elders in the Framingham Study. Am J Public Health 1994;84:351–8.
3. Felson DT, Zhang Y. An update on the epidemiology of knee and hip osteoarthritis with a view to prevention. Arthritis Rheum 1998;41:1343–55.
4. Yelin E, Callahan LF. The economic cost and social and psychological impact of musculoskeletal conditions. National Arthritis Data Work Groups. Arthritis Rheum 1995;38:1351–62.
5. Abadie E, Ethgen D, Avouac B, Bouvenot G, Branco J, Bruyere O, *et al.* Recommendations for the use of new methods to assess the efficacy of disease-modifying drugs in the treatment of osteoarthritis. Osteoarthritis Cartilage 2004;12:263–8.
6. Burstein D, Gray ML. Is MRI fulfilling its promise for molecular imaging of cartilage in arthritis? Osteoarthritis Cartilage 2006;14:1087–90.
7. Eckstein F, Burstein D, Link TM. Quantitative MRI of cartilage and bone: degenerative changes in osteoarthritis. NMR Biomed 2006;19:822–54.
8. Bauer DC, Hunter DJ, Abramson SB, Attur M, Corr M, Felson D, *et al.* Classification of osteoarthritis biomarkers: a proposed approach. Osteoarthritis Cartilage 2006;14:723–7.
9. Kellgren JH, Lawrence JS. Radiological assessment of osteo-arthrosis. Ann Rheum Dis 1957;16:494–502.
10. Altman RD, Hochberg M, Murphy WA Jr, Wolfe F, Lequesne M. Atlas of individual radiographic features in osteoarthritis. Osteoarthritis Cartilage 1995;3(Suppl A):3–70.
11. Altman RD, Gold GE. Atlas of individual radiographic features in osteoarthritis, revised. Osteoarthritis Cartilage 2007;15(Suppl A):A1–A56.
12. Dacre JE, Huskisson EC. The automatic assessment of knee radiographs in osteoarthritis using digital image analysis. Br J Rheumatol 1989;28:506–10.
13. Buckland-Wright JC, Macfarlane DG, Williams SA, Ward RJ. Accuracy and precision of joint space width measurements in standard and macroradiographs of osteoarthritic knees. Ann Rheum Dis 1995;54:872–80.
14. Prakash U, Wigderowitz CA, McGurty DW, Rowley DI. Computerised measurement of tibiofemoral alignment. J Bone Joint Surg Br 2001; 83:819–24.
15. Bruyere O, Henrotin YE, Honore A, Rovati LC, Seidel L, Dardenne C, *et al.* Impact of the joint space width measurement method on the design of knee osteoarthritis studies. Aging Clin Exp Res 2003;15:136–41.
16. Takahashi T, Yamanaka N, Komatsu M, Ogawa Y, Yoshida S, Yamamoto H. A new computer-assisted method for measuring the tibio-femoral angle in patients with osteoarthritis of the knee. Osteoarthritis Cartilage 2004;12:256–9.
17. Linaker CH, Walker-Bone K, Palmer K, Cooper C. Frequency and impact of regional musculoskeletal disorders. Baillieres Clin Rheumatol 1999;13:197–215.
18. Summers MN, Haley WE, Reveille JD, Alarcon GS. Radiographic assessment and psychologic variables as predictors of pain and functional impairment in osteoarthritis of the knee or hip. Arthritis Rheum 1988;31:204–9.
19. Cicuttini FM, Baker J, Hart DJ, Spector TD. Association of pain with radiological changes in different compartments and views of the knee joint. Osteoarthritis Cartilage 1996;4:143–7.
20. Wluka AE, Wolfe R, Stuckey S, Cicuttini FM. How does tibial cartilage volume relate to symptoms in subjects with knee osteoarthritis? Ann Rheum Dis 2004;63:264–8.
21. Boyle RD, Thomas RC. Median filter. In: Boyle RD, Thomas RC, Eds. Computer Vision: a First Course. Blackwell Scientific Publications 1988:32–4.
22. Canny J. A computational approach to edge detection. IEEE Trans Pattern Anal Mach Intell 1986;8:679–714.
23. Hart DJ, Doyle DV, Spector TD. Incidence and risk factors for radiographic knee osteoarthritis in middle-aged women: the Chingford Study. Arthritis Rheum 1999;42:17–24.
24. Jones G, Ding C, Scott F, Glisson M, Cicuttini F. Early radiographic osteoarthritis is associated with substantial changes in cartilage volume and tibial bone surface area in both males and females. Osteoarthritis Cartilage 2004;12:169–74.
25. Kamekura S, Kawasaki Y, Hoshi K, Shimoaka T, Chikuda H. Contribution of runt-related transcription factor 2 to the pathogenesis of osteoarthritis in mice after induction of knee joint instability. Arthritis Rheum 2006;54:2462–70.
26. Yamada T, Kawano H, Koshizuka Y, Fukuda T, Yoshimura K, Kamekura S, *et al.* Carminerin contributes to chondrocyte calcification during endochondral ossification. Nat Med 2006;12:665–70.
27. Brandt KD, Mazzuca SA, Conrozier T, Dacre JE, Peterfy CG, Provvedini D, *et al.* Which is the best radiographic protocol for a clinical trial of a structure modifying drug in patients with knee osteoarthritis? J Rheumatol 2002;29:1308–20.
28. Strand V, Hochberg MC. Study design and outcome measures in osteoarthritis clinical trials. In: Moskowitz RW, Altman RD, Hochberg MC, Buckwalter JA, Goldberg VM, Eds. Osteoarthritis: Diagnosis and Medical/Surgical Management. 4th edn. Philadelphia: Lippincott Williams & Wilkins; 2007:313–25.
29. Mazzuca SA, Brandt KD, Buckwalter KA. Detection of radiographic joint space narrowing in subjects with knee osteoarthritis: longitudinal comparison of the metatarsophalangeal and semiflexed anteroposterior views. Arthritis Rheum 2003;48:385–90.
30. Mazzuca SA, Brandt KD, Dieppe PA, Doherty M, Katz BP, Lane KA. Effect of alignment of the medial tibial plateau and x-ray beam on apparent progression of osteoarthritis in the standing anteroposterior knee radiograph. Arthritis Rheum 2001;44:1786–94.
31. Sanfridsson J, Holje G, Svahn G, Ryd L, Jonsson K. Radiation dose and image information in computed radiography. A phantom study of angle measurements in the weight-bearing knee. Acta Radiol 2000; 41:310–6.
32. Saito T, Koshino T. Distribution of neuropeptides in synovium of the knee with osteoarthritis. Clin Orthop Relat Res 2000;376:172–82.
33. Karachalios T, Zibis A, Papanagiotou P, Karantanas AH, Malizos KN, Roidis N. MR imaging findings in early osteoarthritis of the knee. Eur J Radiol 2004;50:225–30.
34. Felson DT, Chaisson CE, Hill CL, Totterman SM, Gale ME, Skinner KM, *et al.* The association of bone marrow lesions with pain in knee osteoarthritis. Ann Intern Med 2001;134:541–9.
35. Bollet AJ. Edema of the bone marrow can cause pain in osteoarthritis and other diseases of bone and joints. Ann Intern Med 2001;134:591–3.
36. Ravaud P, Giraudeau B, Auleley GR, Drape JL, Rousselin B, Paolozzi L, *et al.* Variability in knee radiographing: implication for definition of radiological progression in medial knee osteoarthritis. Ann Rheum Dis 1998;57:624–9.
37. Wluka AE, Stuckey S, Snaddon J, Cicuttini FM. The determinants of change in tibial cartilage volume in osteoarthritic knees. Arthritis Rheum 2002;46:2065–72.
38. Burgkart R, Glaser C, Hinterwimmer S, Hudelmaier M, Englmeier KH, Reiser M, *et al.* Feasibility of T and Z scores from magnetic resonance imaging data for quantification of cartilage loss in osteoarthritis. Arthritis Rheum 2003;48:2829–35.
39. Cicuttini FM, Jones G, Forbes A, Wluka AE. Rate of cartilage loss at two years predicts subsequent total knee arthroplasty: a prospective study. Ann Rheum Dis 2004;63:1124–7.
40. Raynauld JP, Martel-Pelletier J, Berthiaume MJ, Labonte F, Beaudoin G, de Guise JA, *et al.* Quantitative magnetic resonance imaging evaluation of knee osteoarthritis progression over two years and correlation with clinical symptoms and radiologic changes. Arthritis Rheum 2004;50:476–87.
41. Cicuttini F, Hankin J, Jones G, Wluka A. Comparison of conventional standing knee radiographs and magnetic resonance imaging in assessing progression of tibiofemoral joint osteoarthritis. Osteoarthritis Cartilage 2005;13:722–7.
42. Ledingham J, Regan M, Jones A, Doherty M. Factors affecting radiographic progression of knee osteoarthritis. Ann Rheum Dis 1995;54: 53–8.
43. van Dijk GM, Dekker J, Veenhof C, van den Ende CH. Course of functional status and pain in osteoarthritis of the hip or knee: a systematic review of the literature. Arthritis Rheum 2006;55:779–85.

Transactions of the Materials Research Society of Japan 33[3] 771-774 (2008)

Nanoscale Structured Phospholipid Polymer Brush for Biointerface

Kazuhiko Kitano[1], Ryosuke Matsuno[2,3], Tomohiro Konno[2,3], Madoka Takai[2,3], and Kazuhiko Ishihara[1,2,3]
[1]Department of Bioengineering, [2]Department of Materials Engineering, [3]Center for NanoBio Integration (CNBI), The University of Tokyo, 7-3-1, Hongo, Bunkyo-ku, Tokyo 113-8656, Japan,
Fax: +81-3-5841-8647, e-mail: kitano@mpc.t.u-tokyo.ac.jp

To prepare the biomaterial surface having both lubricity and biocompatibility, we aimed to prove the mechanism of the resistance of friction and protein adsorption with grafting polymer. We prepared poly(2-methacryloyloxyethyl phosphorylcholine) (PMPC) grafted layer using an atom transfer radical polymerization (ATRP) method, which had the advantage of controlling surface structures on nanoscale. From the results of surface characterization, it was confirmed that the thickness of the PMPC grafted layer was 4-10 nm and the conformation of the PMPC grafted layer was brushlike. We investigated the friction properties in air and in water with an atomic force microscopy (AFM). The friction coefficients of the PMPC brush layers were decreased dramatically in water and the resistance of friction depended on the thickness of the PMPC brush layer. We also investigated the protein adhesion properties by measuring the force-distance curves using the AFM cantilever immobilized with a bovine serum albumin (BSA). The adhesion force between the BSA and the PMPC brush layers were markedly reduced and the resistance of the BSA adhesion depended on the thickness of the PMPC brush layer. For resisting both friction and protein adsorption in water, it was a key factor to keep the thick hydrated layer made by the elongated hydrophilic PMPC brush chains.
Key words: phospholipid polymer, polymer brush, atom transfer radical polymerization, atomic force microscopy, lubricity

1. INTRODUCTION

In recent years there has been increasing interest in surface modification with polymers to improve a solid surface properties for biomaterials. Lubricity is one of the essential properties for biomaterials such as artificial joints, blood pump bearings, and catheters. As for artificial joints, the loosening caused by wear between the articulating surfaces is the most serious problem limiting their survival and clinical success. We aimed for obtaining both lubricity and biocompatibility for biomaterial surfaces. We used poly(2-methacryloyloxyethyl phosphorylcholine) (PMPC) as a surface modifier, which is well known for biocompatible polymer whose side chain is composed of phosphorylcholine resembling phospholipid of cell membrane[1-4]. The polymers with MPC units onto the surface of medical devices have already been shown to suppress biological reactions when they are in contact with living organisms. Using the fundamental research results, PMPC are now clinically used on the surfaces of intravascular stents, guide wires, soft contact lenses, and artificial heart[5-7]. Surface grafting of PMPC is excellent method to obtain the biocompatibility[8-10]. We expect that the PMPC grafting also improves lubricity of a solid surface because there are the same phospholipid polar groups on the surface of the human articular cartilage. It has been reported that the PMPC grafting onto the polyethylene liner of the artificial hip joint clearly reduced wear between the articulating surfaces for long term[11,12]. However why the PMPC grafting improves surface lubricity or biocompatibility has not been clear yet. In this study, in order to investigate the surface properties of the PMPC grafted surface, we prepared the nanoscale structured PMPC grafted layer using an atom transfer radical polymerization (ATRP) method, which was famous for preparing well-controlled polymer grafted layer[13,14]. We mainly studied two surface properties on nanoscale. The first is about the friction properties. We measured the friction force of the PMPC grafted surfaces with an atomic force microscopy (AFM). The second is about the protein adhesion properties. We obtained force-distance (*f-d*) curves with a protein immobilized AFM cantilever, and calculated adhesion force of the protein on the PMPC grafted surfaces.

2. EXPERIMENTS

2.1 Surface preparation

2.1.1 Surface-initiator immobilization

SiO_2 coated silicon wafers (Si) were cut into 1.0 cm x 2.0 cm, rinsed sufficiently with acetone and ethanol and treated with oxygen plasma. To prepare the homogeneous monolayer of the initiator on the silicon wafers, monochlorosilane, 3-(2-bromoisobutyryl)-propyl dimethylchlorosilane (BDCS), was used as the surface initiator. We synthesized BDCS as previously described[15]. The cleaned substrates were immersed in a 5 mmol/L toluene solution of BDCS for 24 h. The wafers were removed from the solution, rinsed with methanol, and dried in an argon stream before used for the graft polymerization.

2.2.2 Graft polymerization of MPC

The graft polymerization of MPC on the silicon wafers was performed using an ATRP method. MPC was dissolved in 10mL of dehydrated methanol. Copper bromide (I) (20 mg, 0.135 mmol) and 2,2'-dipyridyl (43 mg, 0.27 mmol) were added with stirring under argon at room temperature. The amount of MPC was changed

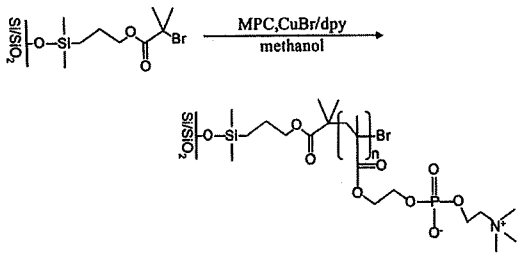

Fig.1 Preparation of the PMPC brush layers on silicon wafer via ATRP.

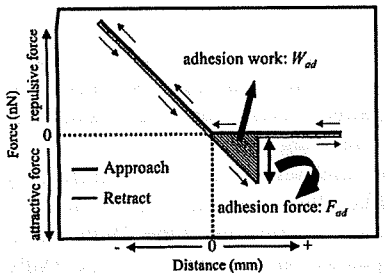

Fig.2 Schematic illustration of a typical *f-d* curve.

variedly in order to control the thickness of the PMPC brush layers. After the solution was stirred for 30 min under an argon gas atmosphere, the BDCS immobilized silicon wafers were immersed into the solution and at the same time ethyl 2-bromoisobutyrate (20 μL, 0.135 mmol) was added as a sacrificial initiator. The polymerization was carried out at room temperature with stirring under an argon gas atmosphere. The silicon wafers were removed from the polymerization mixture after the desired time period. Subsequently, they were extracted with a Soxleht apparatus in methanol for 20h and dried in vacuo at room temperature. The scheme of the reaction is shown in Fig.1.

2.3 Surface characterization

The surface chemical composition was determined by X-ray photoelectron spectroscopy (XPS). Survey scans (0-1100 eV) were performed to identify the C, N, O, and P elements. A take off angle of the photoelectrons was 90°. All binding energies were referenced the C_{1s} peak at 285 eV. The static water contact angles were measured using a goniometer at room temperature. Water droplets of 6 μL were contacted onto the substrates and the contact angles at 10 sec were directly measured by photographic images. The data was collected at 3 positions on each sample. The thickness of the PMPC brush layers in air was measured by ellipsometry. The surface morphology of the PMPC brush layers was observed with an AFM in air. Images were captured in a 1 μm x 1 μm area.

2.4 Interfacial friction measurements

A Nanoscope IIIa AFM (Digital Instruments) was used to characterize interfacial friction properties. Experiments were performed in contact mode in air and in water. V-shaped Si_3N_4 cantilevers with an announced force contact of 0.12 N/m were used. Surface friction data were acquired by scanning in the Trace and Retrace directions by disabling the slow scan axis. The friction voltage signals were corrected and converted to units of force by the previously proposed method[16]. For investigating the friction-load relationship, the scan size was maintained at 2.0 μm and the scan rate at 2.0 Hz, giving a sliding velocity of 8 μm/s. The applied load was varied by changing the vertical deflection of the cantilever. The load was calculated with a method reported previously.[17]. To calculate the load, we measured the *f-d* curve right after every friction imaging. The friction versus sliding velocity measurements was carried out between the sliding velocity of 0.4 μm/s and 488 μm/s. A scan size of 2 μm was used for the measurements.

2.5 Investigation of the protein adhesion properties

2.5.1 Bovine serum albumin (BSA) immobilization onto the AFM cantilever

The BSA-immobilized cantilever was prepared as follows. The oxygen-plasma treated Si_3N_4 cantilever was reacted with an ethanol solution of 3-aminopropyltriethoxysilane (APTES) for 2 h at room temperature, and then rinsed with water and ethanol. The surface silanized with APTES was reacted with a 5 % solution of glutaraldehyde in phosphate buffered saline (PBS) for 3 h, and then rinsed with PBS, followed by immersing in 3 mg/mL BSA in PBS at 37 °C for 3 h. The cantilever was then rinsed with PBS.

2.5.2 Measurements of the *f-d* curves

We measured the *f-d* curves in PBS (pH = 7.4) using the BSA-immobilized AFM cantilever and obtained the adhesion properties between the BSA and the PMPC brush layers. Fig.2 shows a typical *f-d* curve for an AFM cantilever contacted with a solid surface. The maximum normal deflection of the retracting curve was defined as adhesion force, F_{ad}, and the area framed by approaching curve and retracting curve was defined as adhesion work, W_{ad}. We used these two parameters for comparing adhesion properties. More than two *f-d* curves were obtained at one location through repeated cantilever approach/retract cycles, and the measurements were also repeated at more than five locations on each sample.

3. RESULTS AND DISUCUSSIONS

3.1 Surface characterization

The grafting of PMPC on the silicon wafers was confirmed using XPS. The peaks in the carbon atom region (C_{1s}) at 286 eV and 289 eV indicated the ether bond and the ester bond, respectively, and those in the nitrogen atom region (N_{1s}) at 403 eV and phosphorus atom region (P_{2p}) at 133 eV were specific to the phosphorylcholine group in the MPC unit. The results of the contact angle and the dry thickness are shown in Fig.3. The static water contact angles on the PMPC brush layers were about 10-25°, which was 20-30 % of those on the unmodified Si. The PMPC grafting greatly increased hydrophilicity, and a very little introduction of the PMPC chains made dramatic effects on the wettability by water. The thickness of the PMPC brush layers was increased with an increase in polymerization degree. We controlled the thickness of the PMPC brush layers by changing the amount of the MPC monomer in the polymerization solution. The dry thickness of the PMPC brush layers was used to estimate the graft density σ by,

$$\sigma = h\rho N_A / M_n$$

where h is the layer thickness determined by ellipsometry, ρ is the density of dry polymer layer